Astron. Astrophys. 298, 743–766 (1995)

ASTRONOMY AND ASTROPHYSICS

The CO emission of ring galaxies

C. Horellou[1] **F. Casoli**[21], **F. Combes**[12], **and C. Dupraz**[2]

[1] DEMIRM, Observatoire de Paris, 61 avenue de l'Observatoire, F-75014 Paris, France
[2] Ecole Normale Supérieure, 24 rue Lhomond, F-75231 Paris Cedex 05, France

Received 24 January 1994 / Accepted 2 December 1994

Abstract. Using the 15m SEST and 30m IRAM telescope we have observed 16 ring galaxies in the ^{12}CO(1-0) transition and detected 14. Six ring galaxies have been detected in the ^{12}CO(2-1) line. The Cartwheel, often considered as the prototype of ring galaxies, has not been detected. We suggest that the weak CO emission of this galaxy is due to its low metallicity. The observations do not exclude the possibility that the Cartwheel may be H_2 rich and actively forming stars. We also present new HI detections of six rings. We have compared the CO emission of the ring galaxies with that of the distance-limited sample of Sage (1993a,b) and found that ring galaxies are bright in CO compared to normal galaxies. If the standard conversion factor from CO emissivities into H_2 column densities holds for ring galaxies, this suggests that a large amount of molecular gas is available for star formation and that ring galaxies are actively forming stars. This result is in agreement with the high far-infrared luminosities of ring galaxies. We have also observed two Hoag-type objects in CO but have detected neither of them.

Key words: galaxies: evolution – galaxies: formation – galaxies: ISM – radio lines: galaxies

1. A peculiar class of interacting galaxies: the ring galaxies

Interacting or merging galaxies often exhibit high rates of star formation. Indeed, close tidal encounters can strongly affect the interstellar medium of the colliders and trigger strong bursts of star formation on a timescale of a few 10^8 years (e.g., Noguchi & Ishibashi 1986; Hernquist 1989). Observations generally show that such starbursts are located near the nuclei of the two galaxies. However, a peculiar class of interacting objects, the ring galaxies, provides an example of coherent starbursts on a scale often larger than 10 kpc. These galaxies appear as relatively well defined, crisp rings that may be enucleated (Theys & Spiegel 1976). A companion is frequently visible near the minor axis of the ring galaxy. Numerical simulations have demonstrated convincingly that such a ring-like structure develops when a galaxy collides head-on with a disk-like companion (Lynds & Toomre 1976; Theys & Spiegel 1977). The galaxy in transit exerts a brief inward pull on the stars of the target galaxy, which will execute radial harmonic oscillations in addition to their initial circular motion. This results in the formation and propagation of a ring wave through the target disk which is accompanied by a strong burst of star formation (Struck-Marcell & Appleton 1987). Optical and infrared observations show that most rings are very blue, and exhibit low-excitation emission lines (Theys & Spiegel 1976). Their average far-infrared luminosity L_{FIR}, far-infrared to blue luminosity ratio L_{FIR}/L_B and colour temperature T(60μm/100μm) are also significantly greater than those of normal galaxies (Appleton & Struck-Marcell 1987a).

The interstellar medium of ring galaxies is poorly known. Although true ring galaxies are not very numerous, no systematic study of their atomic and molecular gas properties has been undertaken. This may be because many rings have small angular sizes so that they can hardly be resolved by single-dish telescopes either at centimeter or millimeter wavelengths. On the other hand, they are often too faint to be detectable with interferometers. The work presented here is a first step towards a better knowledge of the molecular gas content in these peculiar objects. Since the dense cores of molecular clouds are the places where stars form, observations of the molecular phase of the interstellar medium are important to get insight on the star formation activity of these galaxies. Using the SEST 15m and IRAM 30m telescopes, we have made a survey of the ^{12}CO(J=1–0) emission of 16 ring galaxies. We have used the CO data to derive the molecular gas content of the galaxies and in some cases to obtain information on the spatial distribution of the molecular gas. We have made additional HI observations of six ring galaxies using the Nançay , Parkes and Arecibo radiotelescopes.

Table 1 gathers optical and far-infrared data of the sample galaxies. Eleven out of the 16 ring galaxies have been taken from the list of Appleton & Struck-Marcell (1987a). The sample contains nearby galaxies such as AM1045–245 at a velocity of 3730 km s^{-1} as well as very distant objects such as the Sextans

* Present address: Chalmers University of Technology, Onsala Space Observatory, 439 92 Onsala, Sweden

Table 1. The sample

Name	Other names	α (1950)	δ (1950)	V_{hel} km s^{-1}	Size ("x")	B^0_T	ref B^0_T	$S_{60\mu m}$ (Jy)	$S_{100\mu m}$ (Jy)	T_{FIR} (K)
IC4448	AM1434-783, E022-G002	14:34:36.0	-78:35.7	4580	60x48	13.25	(1)	2.32	5.02	35.1
AM064-741	Lindsay-Shapley,E34-G11, A0644-74	06:44:21.5	-74:11:27	6611	95x50	12.98	(1)	1.42	4.2	31.0
AM0530-421	E306-G09, Fairall 1135	05:30:06.7	-42:11:56	14500	60x60	13.82	(1)	0.55	1.86	29.4
Vela	AM1006-380, E316-G32	10:06:56.7	-38:09:49	4845	70x50	12.76	(1)	1.06	3.65	29.2
Cartwheel	A0035-34, VV784, E350-G40	00:35:14.3	-33:59:27	8934	74x60	13.86	(3)	0.65	1.6	33.3
AM1045-245	E501-G100, NGC 3393	10:46:00.0	-24:53:48	3730	132	12.66	(1)	2.38	3.94	39.6
NGC985	Mrk1048, VV285	02:32:10.6	-09:00:21.7	12948	39x23	13.89	(1)	1.44	2	43.0
Sextans	IRAS09595-0755	09:59:30.9	-07:55:15	16500	20	15.5	(4)	0.92	1.5	39.8
Arp147	IC298A/B, IZw11, VV787	03:08:43.5	01:07:30.9	9665	19x16	15.7	(5)	0.98	1.9	36.8
IIZw28	A0459+03, VV 790b	04:59:04.1	03:30:06	8611	14x10	14.94	(6)	<0.50	< 1.00	
IRAS20210		20:21:02.5	11:21:52	16900		15.83	(7)	3.31	2.78	56.4
Arp119	Kar29, Mrk984, UGC849, VV347	01:16:45.3	12:11:03	14265	84	14.2	(1)	0.73	1.65	34.5
IIHz4	A0855+37, CGCG180-023	08:55:23.0	37:16:50	12830	29x32	15.6	(7)	<0.50	< 1.00	
Arp143	NGC2444/45, VV117	07:43:32.7	39:08:19	4020	85x70	13.58	(1)	3.39	6.32	37.5
Arp148	Mayall's Object=A1101+41	11:01:05.8	41:07:10.2	10350	22x15	15.05	(9)	6.06	10.66	38.5
Arp145	A0220+41A/B, UGC1840, VZw229	02:20:00.4	41:08:38.3	5178	58x40	13.61	(1)	0.83	1.83	34.9
NGC6028 *	UGC10135, IZw133	15:59:15.8	19:29:49	4480	65x65	14.21	(1)	<0.50	< 1.00	
Hoag's object *		15:15:01.0	21:46:00	12735	36x36	15.8	(8)	<0.50	< 1.00	

* Hoag-type objects, not included in the statistical analysis

References for B^0_T: (1) de Vaucouleurs et al .1991; (2) Lyon Extragalactic Database; (3) Marcum et al. 1992; (4) Davoust et al. 1991; (5) Zwicky et al. 1961-1968); (6) Gordon and Gottesman 1981; (7) NASA Extragalactic Database; (8) Wakamatsu 1990; (9) Appleton and Struck-Marcell 1987

The dust temperatures (last column) have been derived from the IRAS fluxes at 60 and 100 μm by fitting a black body and assuming that the dust emissivity is proportional to λ^{-1}

IIZw28 has been detected by IRAS at 60 μm only (IRAS Point Source Catalogue). We derived the S_{100} flux by assuming a S_{100}/S_{60} ratio of 2.25 (Appleton and Struck-Marcell 1987)

ring at 16500 km s^{-1}. We have observed well-studied objects such as the Cartwheel and the Vela ring, but also galaxies of which almost nothing is known (e.g., IRAS20210+1121). Four galaxies of the sample (NGC 985, Sextans, IRAS20210 and AM1045-245) host a Seyfert nucleus. Out of the 16 objects, one was not detected by IRAS at either 60 or 100 μm (IIHz4), and one (IIZw28) was detected at 60 μm only.

We expect all these objects to be true collisional rings and not "ringed" galaxies (Buta 1986) where the ring is a less prominent and more symmetric feature probably due to the outer Linblad resonance, or "Hoag-type object" (Hoag 1950, see Fig. 19). The latter appear as elliptical-like galaxies with a prominent outer ring. They probably have not been induced by a collision since they are almost perfectly circular and moreover no nearby companion is visible. The physical phenomenon which gives birth to such a structure is not well established. Brosch (1985) proposed that the ring of Hoag's object may have formed as the result of a bar instability in the galactic disk but no barred structure has been observed; Schweizer et al. (1987) proposed that gas has been transferred from a companion galaxy and accreted onto an elliptical galaxy and settled into a ring as in polar ring galaxies. We have observed two Hoag-type objects in CO: Hoag's object itself and NGC 6028.

The content of this article is as follows: Sect. 2 gives some observational parameters. In Section 3, we discuss the results for individual sources. Section 4 contains a general discussion of the molecular content of ring galaxies compared to other CO surveys. Observations of two Hoag-type objects are presented in Sect. 5. The conclusions of the article are gathered in Sect. 6.

2. Observations

2.1. General characteristics

Let us give first some general characteristics of the CO data used in this article (see Table 2). The temperature scale will be the main-beam temperature scale $T_{mb} = T_A^*/\eta_{mb}$, which should be appropriate for sources which approximately fill the beam. We use the notation:

$I_{10} = \int T_{mb}[^{12}CO(1-0)]dv$,

and $I_{21} = \int T_{mb}[^{12}CO(2-1)]dv$.

The uncertainties in the integrated intensities have been computed by using the same method as in Sage (1993a, b); they are the quadratic sum of errors due to noise in the spectrum and in the determination of the baseline:

$$\Delta I = \sigma_{rms}\, \Delta v_i\, ([\Delta v_c/\Delta v_i]^{1/2} + [\Delta v_c/\Delta v_b]^{1/2})$$

where Δv_i = velocity range over which the spectrum was integrated, Δv_c = the smoothed channel width and Δv_b the velocity range over which the baseline was fitted.

We calculate molecular hydrogen masses using the galactic conversion factor:

$N(H_2) = 2.3\ 10^{20}\ I_{10}$ (Strong et al. 1988).

For the SEST 43" beam this converts into

Table 2. Observational data

Name	Telescope	Line	Observed positions (",")	v(line) km s^{-1} (1)	Δv km s^{-1} (2)	$\int T\,dv$ (3)	M(H_2) (10^9 $M_\odot$) (4)
IC4448	SEST	CO(1-0)	(0,0)	4518	78	3.6±0.8	1.7
-	Parkes	HI	(0,0)	v_{rad}=4491 ->v_{opt}=4559	103	5.2±0.4a)	
AM064-741	SEST	CO(1-0)	Map with 45" sampling (see Fig.2)				
			(0,0)	6307	162	2.0±0.6	1.7
			(0,+45)	6289	53	0.7±0.5	0.6
			(+45,0)	6199	81	1.0±0.4	0.9
			Total				3.2 a)
AM0530-421	-	CO(1-0)	(0,0) (+20,0) (-20,0) (+20,0) (0,+20) (-20,+20) (+20,-20) (0,-20) (-20,-20) (0,-45) (see Fig. 3)				
				14565	117	0.6±0.1	5.2 b)
-	Parkes	HI	(0,0)	v_{rad}=13888 ->v_{opt}=14562	126	5.7±0.3	
Vela	SEST	CO(1-0)	(0,0)	4852	34	2.6±0.5	1.4
-	-	CO(2-1)	(0,0)	4859	28	3.5±0.9	
Cartwheel	-	CO(1-0)	5-point map with 45" sampling				
			(-29,+7.7) (-7.7,-29)	ND		<0.22	<1.5 c)
AM1045-245	-	CO(1-0)	(0.0)	3734	171	1.4±0.6	<0.4
-	Nançay	HI	(0,0)	3747	145	8.1±0.2	
NGC985	IRAM 30m	CO(1-0)	Map with 10" sampling (see Figs 7c and d)				
			(-30,0)	13038	37	3.5±1.0	
			(-20,0)	13021	70	5.2±0.7	
			(-10,0)	12990	105	6.8±0.9	
			(0,0)	12885	253	8.2±0.9	
			(-30,+10)	13025	73	7.3±0.2	
			(-10,+10)	12984	130	13.7±2.1	
			(0,+10)	12812	305	7.6±0.9	
			Total				12.0 d)
-	-	CO(2-1)	(-20,0)	12999	77	8.6±2.1	
			(-10,0)	12974	119	4.4±1.4	
			(-20,+10)	13003	36.4	6.3±1.3	
			(-10,+10)	12989	72	4.4±0.7	
			(-20,+20)	13033	36.7	6.7±2.7	
Sextans	-	CO(1-0)	Map with 10" sampling (see Figs 8c and d)	16385	216	7.3±1.4	11.5 e)
-	-	CO(2-1)	-	ND			
-	Nançay	HI	(0,0)	16591	133	1.6±0.1	

(1) Line centroid. Optical definition of the velocities, except for IC4448 and AM0530-421. ND: not detected (2) Linewidth (3) Integrated intensity in K km s^{-1} for the CO(1-0) and CO(2-1) line and in Jy km s^{-1} for the HI line. a) IC4448: the uncertainty in the HI integrated intensity has been estimated from the spectrum with a total velocity range of 1600 km s^{-1} and not from the spectrum shown in Fig. 1c where the velocity range is the same as that of the CO spectrum for clarity (4) Total molecular gas mass and procedure used in the computation when the galaxy was mapped: a) AM064-741: addition of the H_2 masses derived from the CO(1-0) spectra at (0,0), (45,0), (0,45). b) AM530-421: 10-point average spectrum. Map area: 2x(45")^2. c) Cartwheel: upper limit computed from the r.m.s in the CO spectra and the HI linewidth (355 km s^{-1}, Mebold et al. 1977). Assumption that the emission is extended on about 80 arcsec scale. d) NGC985: the CO flux integrated over the whole galaxy has been computed from the contour map (Fig. 7b). e) Sextans: from the spectrum at the (0,0) position

Table 2. (continued)

Name	Telescope	Line	Observed positions (",")	v(line) km s^{-1} (1)	Δv km s^{-1} (2)	$\int T_{mb} dv$ (3)	M(H_2) (10^9 $M_\odot$) (4)
Arp147	IRAM 30m	CO(1-0)	(0,0) (+9,-4) (+4,+9) (-5,+13) (-9,+4) (+13,+5)				
				9603	191	2.2±0.4	2.2 f)
IIZw28	-	CO(1-0)	(0,0)	ND			0.85
IRAS20210	-	CO(1-0)	(0,0)	16951	320	2.5±0.5	4.1
-	-	CO(2-1)	-	16960	125	2.8±2.0	
Arp119	-	CO(1-0)	(0,0)	14266	38	3.4±0.3	4.1
-	-	CO(2-1)	-	14269	52	2.8±0.6	
-	Arecibo	HI	-	14246	178	1.4±0.2	
IIHz4	IRAM 30m	CO(1-0)	Map with 10" sampling (see Fig. 13)	12848	36	0.7±0.3	1.3 g)
-	-	CO(2-1)	-	12831	40	1.1±0.3	
Arp143	-	CO(1-0)	Map with 20" sampling (see Fig. 16)				
			(0,0)	3990	151	13.3±1.3	
			(+10,-10)	3942	150	8.5±2.6	
			(-10,-10)	4028	149	6.1±2.4	
			(-10,+10)	3978	138	16.5±2.1	
			(0,+20)	4017	91	7.1±1.5	
			(+20,0)	3952	323	4.7±1.2	
			(0,-20)	4018	244	6.5±1.5	
			Total				3.0 h)
-	-	CO(2-1)	(0,+20)	4016	64	6.8±1.7	
Arp148	-	CO(1-0)	Map with 10" sampling (see Fig. 17)	10361	126	18.3±1.9	11.5 i)
Arp145	-	CO(1-0)	Map with 10" sampling (see Fig. 18)	5268	168	3.5±0.3	2.3 j)
-	Nançay	HI	(0,0)	5307	243	1.3±0.4	
Hoag's object*	IRAM 30m	CO(1-0)	(0,0)	ND			< 0.7
NGC6028 *	-	CO(1-0)	(0,0)	ND			< 0.045

* Hoag-type objects, not included in statistics (4) Total molecular gas mass and procedure used in the computation when the galaxy was mapped: f) Arp147: 6-point average spectrum. Map area: $(30")^2$ g) IIHz4: 9-point average spectrum. Map area: $2x(23")^2$ h) Arp143: the CO flux integrated over the whole galaxy has been computed from the contour map (Fig. 13b). i) Arp148: from the spectrum at the (0,0) position. j) Arp145: 11-point average spectrum. Map area: $(45")^2$

$$M(H_2)\,(M_\odot) = 1.25\,10^5\ I_{10}\ (D/1\ \mathrm{Mpc})^2 \text{ in one beam,}$$

where D is the distance to the galaxy in Mpc. For the IRAM 22" beam, this gives

$$M(H_2)\,(M_\odot) = 3.28\ 10^4\ I_{10}\ (D/1\ \mathrm{Mpc})^2 \text{ in one beam,}$$

Note that throughout this paper we shall use a Hubble constant $H_o = 75$ km s^{-1} Mpc^{-1}.

Several sample objects have been mapped. To compute their total H_2 mass, we have in some cases produced an average spectrum over the whole map and computed the corresponding mass using the map surface instead of the beam area. The map area is indicated in Table 2. For NGC 985 and Arp 143, the map is more extended and we have computed the CO flux integrated within the 1 K km s^{-1} contour in the map using the command POLYGON in the data reduction package CLASS.

The conversion factor from CO(1-0) line areas to H_2 column densities is an empirical value determined in the disk of our galaxy. It is clear that this value could be wrong for disturbed and perturbed objects such as the ring galaxies. In the absence of any information on the conversion factor in external galaxies and its dependance upon various factors such as the metallicity, the gas structure and its temperature, we have chosen to use the standard value. When a galaxy was not detected in CO, we have used the HI linewidth in conjunction with the average noise per channel in the CO spectra to produce an upper limit (see Tables 2 and 3).

The HI masses are related to the HI integrated intensities F(HI) (in Jy km s^{-1}) by:

$$M(HI)\,(M_\odot) = 2.36\,10^5\ F(HI)\ (D/1\ \mathrm{Mpc})^2$$

where D is the distance to the galaxy in Mpc.

Finally, let us note that all the velocities quoted here are heliocentric, using the optical definition $v_{opt} = cz = c\Delta\lambda/\lambda$ except for the two HI spectra obtained at Parkes that have the

Table 3. Blue and far-infrared luminosities and gas masses

Name	D (Mpc) (a)	L_{FIR} (10^{10} L_o) (b)	L_B (10^{10} L_o) (c)	L_{FIR}/L_B	M(HI) (10^9 M_o)	Reference HI (d)	$M(H_2)$ (10^9 M_o)	$M(H_2)/M(HI)$	$M(HI)/L_B$ (M_o/L_o)	$M(H_2)/L_B$ (M_o/L_o)	$L_{FIR}/M(H_2)$ (L_o/M_o)
IC4448	61	2.27	2.91	0.78	4.4	(8)	1.70	0.40	0.15	0.058	13.3
AM064-741	88	3.73	7.77	0.48			3.20			0.041	11.6
AM0530-421	193	7.9	17.2	0.46	46.0	(8)	5.20	0.11	0.27	0.030	15.2
Vela	65	1.76	5.11	0.34	0.7	(1)	1.42	2.03	0.01	0.028	12.4
Cartwheel	119	2.66	6.31	0.42	33.0	(2)	< 1.50	< 0.05	0.52	< 0.024	> 17.8
AM1045-245	50	1.34	3.32	0.40	4.6	(8)	0.47	0.1	0.14	0.014	28.5
NGC985	173	9.02	12.9	0.70	< 5.8	(3)	12.0	> 2.08	0.04	0.093	7.5
Sextans	220	11.1	4.75	2.34	18.0	(8)	11.5	0.64	0.38	0.242	9.6
Arp147	129	3.99	1.36	2.94	5.2	(4)	2.20	0.42	0.38	0.162	18.1
IIZw28	115	< 1.65	2.17	< 0.76	2.3	(4)	< 0.85	<0.37	0.11	<0.039	
IRAS20210	225	34.4	3.68	9.35			4.10			0.111	83.9
Arp119	190	7.15	11.8	0.61	12.0	(8)	4.05	0.34	0.10	0.034	17.6
IIHz4	171	< 3.65	2.62	< 1.39	8.3	(4)	1.30	0.16	0.32	0.050	> 28.1
Arp143	54	2.36	1.65	1.43	6.6	(7)	3.00	0.45	0.40	0.181	7.9
Arp148	138	26.7	2.83	9.43			11.5			0.406	23.2
Arp145	69	1.05	2.67	0.39	1.4	(8)	2.30	1.64	0.05	0.086	4.6
NGC6028*	60	< 0.45	1.15	< 0.39	1.6	(6)	<0.045	< 0.03	0.14	< 0.004	
Hoag's object*	170	< 3.61	2.15	< 1.68	8.0	(7)	< 0.70	< 0.09	0.37	< 0.033	

* Hoag-type objects, not included in the statistics

a) Distance to the galaxy (H_o=75 $kms^{-1}Mpc^{-1}$)

b) The far-infrared luminosities have been derived from the IRAS fluxes at 60 and 100 μm by fitting a black body and assuming that the dust emissivity is proportional to λ^{-1}

c) The intrinsic blue luminosities L_B have been derived from the blue magnitudes B^o_T using the following relation: $\log(L_B/L_o) = 12.192 - 0.4\ B^o_T + \log(D/1Mpc)^2$ (consistent with the blue magnitude for the Sun M_{Bo}= 5.48)

d) Reference for the HI data: 1) Martin, private communication; 2) Mebold et al. 1977; 3) Heckman et al. 1978; 4) Jeske 1986; 5) Giovanelli et al. 1981; 6) Schweizer et al. 1987; 7) Gallagher et al. 1981; 8) this work

radio convention $v_{rad} = -c\Delta\nu/\nu$. Optical and radio velocities are related by:

$$v_{rad} = v_{opt}/(1+v_{opt}/c)$$

2.2. *Southern objects*

The CO observations of the southern objects (that is, all objects of negative declination except NGC 985) were carried out during several observing runs between 1988 and 1993 using the 15 m Swedish-ESO Submillimeter Telescope (SEST) at La Silla, Chile (Booth et al. 1989). At 115 GHz [^{12}CO(1-0)], the telescope half-power beamwidth is 43" and the main-beam efficiency η_{mb} is 0.74. At 230 GHz [^{12}CO(2-1))], they are respectively 22" and 0.60 (after October 1990; before June 1990 this factor efficiency had the value 0.54, and 0.75 in between; Nyman, private communication). Pointing errors were about 5" r.m.s. At 115 GHz, we used a Schottky receiver in single sideband mode with T_{rec} = 300 K ; T_{sys} was between 400 and 500 K. At 230 GHz, the receiver had a single-sideband temperature of 700 - 900 K; the system temperature varied from 1300 to 2000 K depending on the frequency and the weather conditions. We used a 6 Hz dual beam-switching procedure with two symmetrical reference positions offset by 12' in azimuth. The backends were two acousto-optical spectrometers with a channel width of 691 kHz and 679 kHz respectively.

Two galaxies (IC 4448 and AM0530-421) were observed in HI in September 1994 with the 64-m Parkes antenna, Australia. The Parkes antenna has a beamwidth of 15' at λ21 cm, a sensitivity of 0.63 K Jy^{-1}, and was equipped with a cryogenically cooled receiver with a system temperature of about 40 K for each linear polarization. The backend was a 2048 channel autocorrelator, with a bandwith of 16 MHz. The galaxies were observed by position-switching between source and empty sky. The reference position was taken 5' time away from the source in right ascension. The data were reduced using the Spectral Line Analysis Package (SLAP).

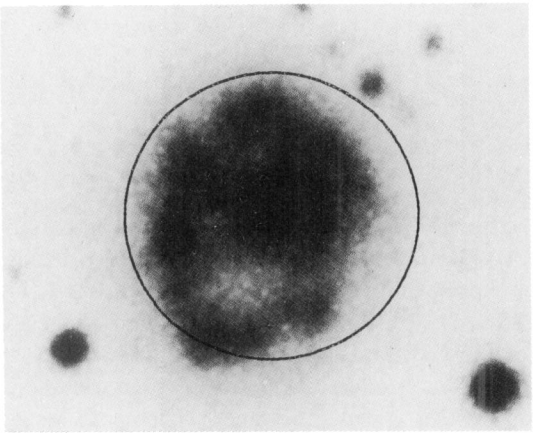

Fig. 1a. Optical photograph of IC 4448 (Arp & Madore 1985, hereafter AM)

To improve the signal to noise ratio the data were smoothed to the resolution indicated in the figure captions. Only lin-

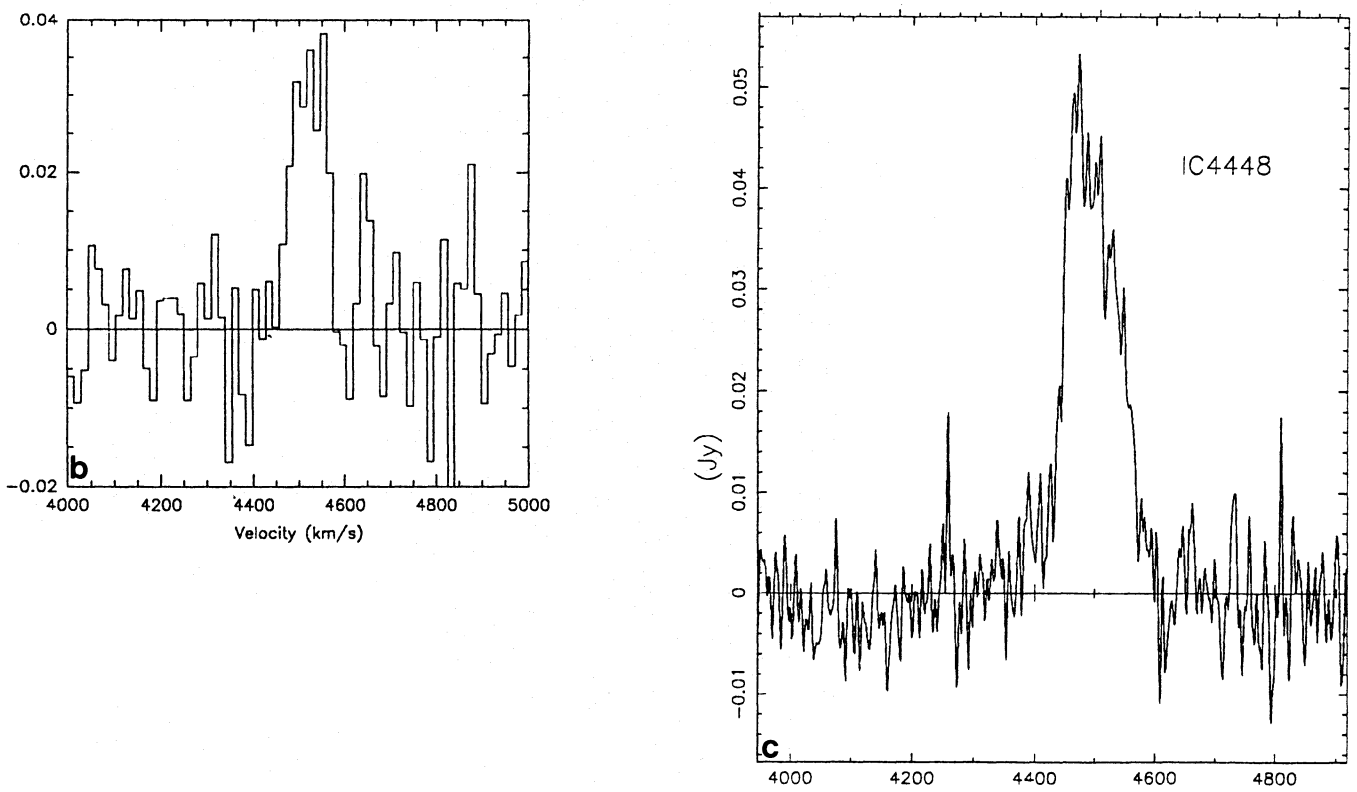

Fig. 1b. CO(1-0) spectrum obtained towards the centre position of IC 4448. The velocity resolution is 14.7 km s^{-1}. **c** HI spectrum of IC 4448. The velocity resolution is 6.4 km s^{-1}. The velocity convention is the radio one for the HI spectrum

ear baselines were subtracted except for the HI spectrum of AM0530-421 where a third order polynomial has been fitted.

2.3. Northern objects

The other galaxies have been observed between 1990 and 1993 with the IRAM 30 m telescope at Pico Veleta near Granada, Spain. The telescope beamsize is 22" at 115 GHz [^{12}CO(1-0)], and 13" at 230 GHz [^{12}CO(2-1)]. The main-beam efficiency hmb is 0.56 at 115 GHz and 0.45 at 230 GHz. The data presented in this paper were collected when the weather conditions were fairly good, with a typical water vapour content of 3 mm or less, yielding zenith opacities around 0.2 at 115 GHz, and 0.1–0.2 at 230 GHz. Pointing was checked at least every two hours by broadband continuum observations of planets and radiocontinuum sources: the errors were less than 5" r.m.s. The system temperature and the antenna temperature corrected for telescope and atmospheric losses T_A^* were calculated by chopper wheel calibrations. Typical system temperatures are 500–1000 K for ^{12}CO(1-0) and 900–1100 K for ^{12}CO(2-1).

The J=1–0 and 2–1 transitions of the CO molecule were observed simultaneously, using a beam splitter to divide the beam in two orthogonal polarizations, each detected by a SIS receiver. The backends consisted of two filterbanks of 512 contiguous 1 MHz channels, providing a velocity resolution of 2.6 km s^{-1} and a total velocity coverage of 1331 km s^{-1} at 115 GHz, and 1.3 km s^{-1} and 657 km s^{-1} at 230 GHz. We used a nutating subreflector switching procedure with a beam throw of 4'. Each five or eight-minute scan began by a chopper-wheel calibration on an ambient-temperature load; additional calibrations on a cold load (liquid nitrogen) were performed every 15 minutes. The baselines were generally very flat owing to the use of the nutating subreflector: only linear baselines were subtracted.

Three galaxies (AM1045-245, Sextans and Arp 145) have been observed in the HI line with the Nançay radiotelescope (see tables 2 and 3). The half-power beamwidth is 4' (E-W) by 21' (N-S). The dual channel receiver had a system temperature of about 50K. The backend was a 1024 channel autocorrelator spectrometer. Total-power mode was used, with a reference position 30' away from the sources. To compute HI column densities, the antenna temperatures T_A^* have been converted into flux densities S_ν by using the conversion ratio appropriate to the declination of the sources (Fouqué et al. 1990).

3. Observational results: individual galaxies

The results are presented in Tables 2 and 3. The objects are sorted by increasing declination. An optical picture of every galaxy is presented. North is to the top, east to the left. A circle representing the resolution of the CO observations has been superimposed on each optical photograph, approximatively centered at the centre position of the galaxy. The superposition is rather uncertain because no coordinates were usually given on

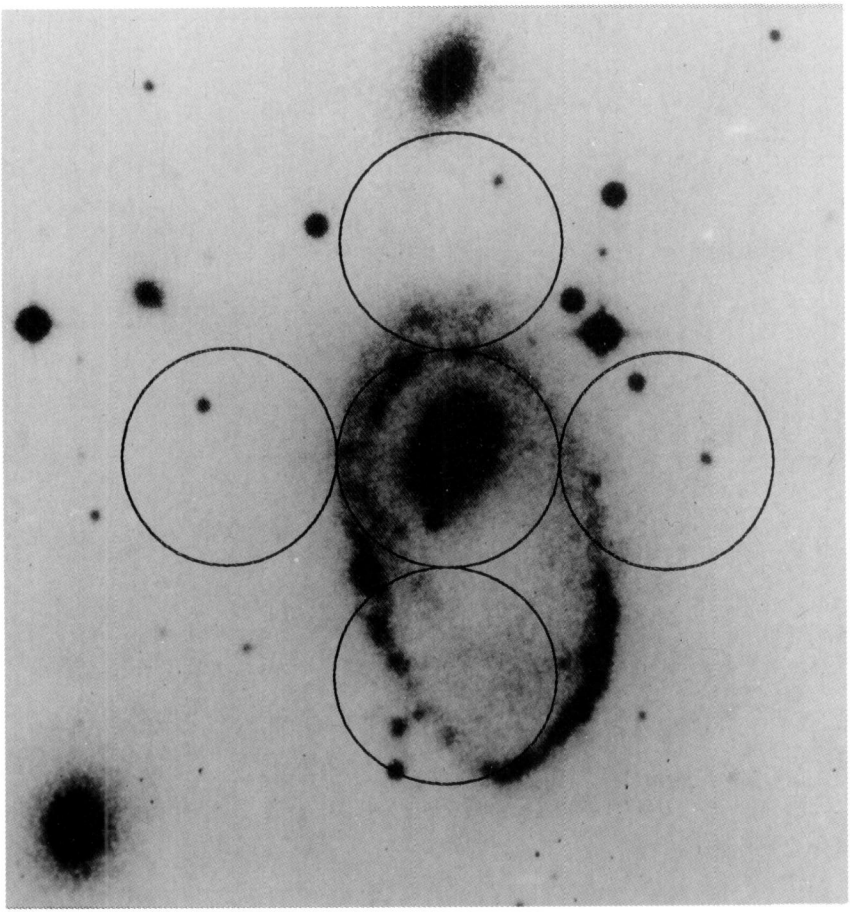

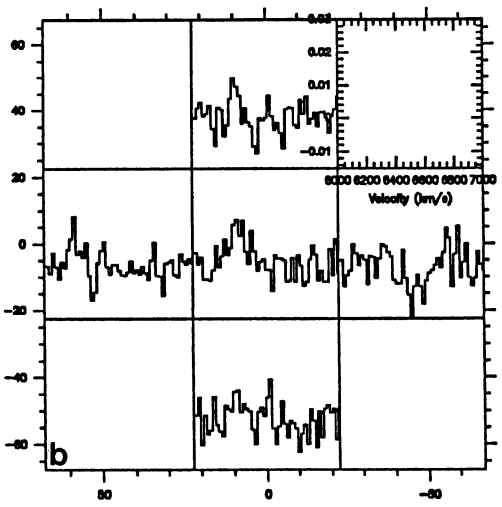

Fig. 2a. Optical photograph of AM064-741 (taken from AM). **b** CO(1–0) map of AM064-741 at 45" sampling (full-beam of SEST at 115 GHz). The velocities range from 6000 to 7000 km s^{-1} and the main-beam temperatures from -0.015 to 0.03 K. The velocity resolution is 20.0 km s^{-1}

the optical pictures; moreover, there are uncertainties in the position of the centre of the galaxy itself (NED database).

3.1. IC 4448

IC 4448 is a knotty ring with an offset nucleus (Fig. 1). Both the CO(1-0) and the HI spectrum obtained towards the centre position of IC 4448 are narrow (Δv = 85 and 126 km s^{-1} respectively). The corresponding H_2 and HI masses are 1.7 10^9 and 4.4 10^9 $M_\odot$.

3.2. AM064-741 (= Lindsay-Shapley ring)

At the time of its discovery by Lindsay & Shapley (1960), the nature of AM064-741 was not clear. It was identified as a ring galaxy by Graham (1974). AM064-741 has three elliptical companions with very close velocities (Fig. 2). The presence of a faint plume of material between the ring and the companion near the minor axis strengthens the suspicion that it is the intruder. The ring is elliptical and contains a prominent nucleus located near the focus position. In fact, the ring is better described by a tightly wound spiral arm that can be followed on almost two revolutions. It is brighter at some locations where there are condensations of blue stars and associated HII regions. Kinematical studies of AM064-741 have shown that the ring is rotating about three times as fast as it is expanding, as predicted by the models (Few et al. 1982).

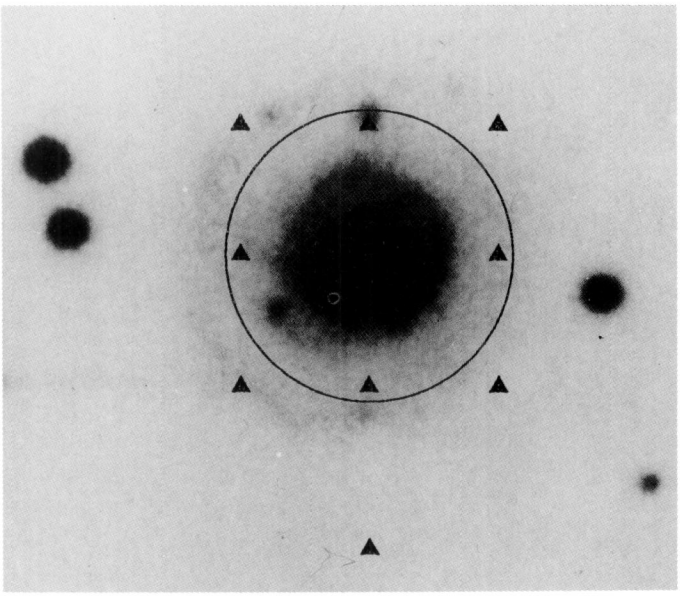

Fig. 3a. Optical photograph of AM0530-421 (taken from AM). The circle represents the 43" SEST beam, the triangles indicate the positions observed

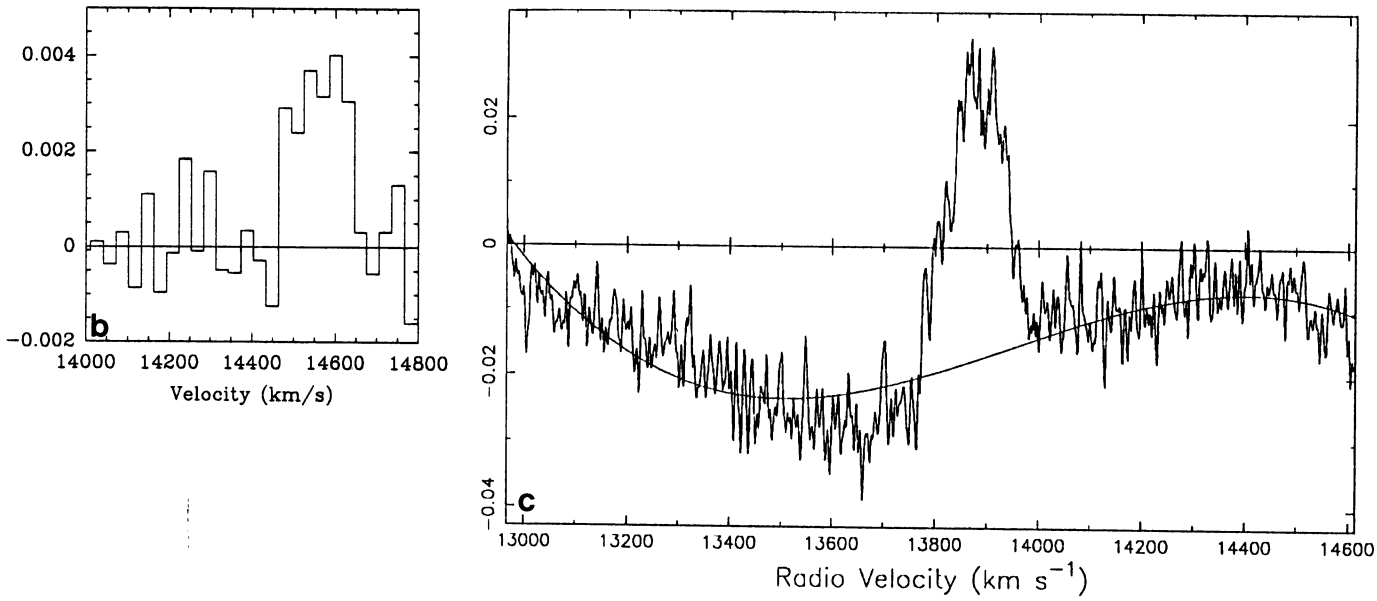

Fig. 3b. CO(1-0) spectrum of AM0530-421 obtained by averaging 10 spectra (see table 2 for details). The velocity resolution is 30.2 km s^{-1}. **c** HI spectrum of AM0530-421. The velocity resolution is 5.0 km s^{-1}. The velocity convention is the radio one for the HI spectrum (v_{rad}= 13890 km s^{-1} corresponds to v_{opt}= 14565 km s^{-1}). The velocity of the CO line agrees with that of the HI

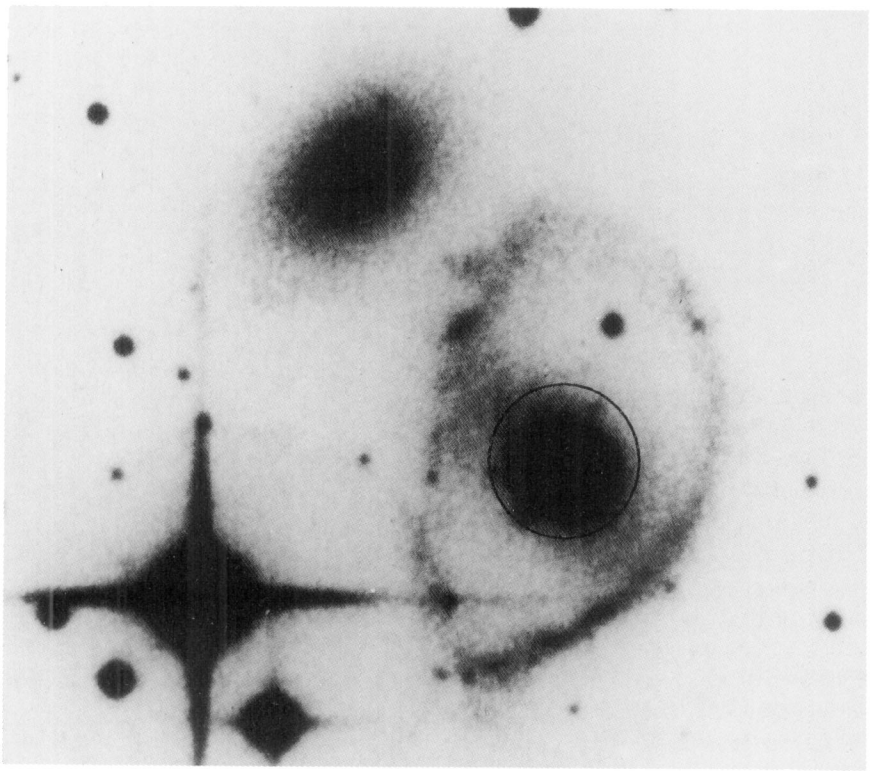

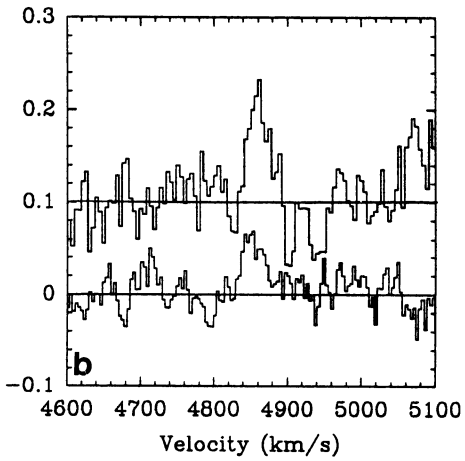

Fig. 4a. Optical photograph of Vela (taken from AM). The circles on the optical picture represent the CO(1-0) and CO(2-1) beams (43" and 22" which corresponds to 13.5 and 6.9 kpc respectively at the distance of Vela). **b** CO(1-0) spectrum and CO(2-1) spectrum (offset by 0.1K for clarity) obtained towards the centre position of Vela. The velocity resolution is 4.6 km s^{-1} for both lines

We have detected CO(1–0) emission at the centre position of AM644-741, at 45" east and at 45" north to it (Fig. 2). From addition of those three spectra, we derive a total H_2 mass of 3.2 10^9 $M_\odot$.

3.3. AM0530-421

AM0530-421 appears as a diffuse ring of about one arcminute diameter with a prominent nucleus (Fig. 3). It was observed by Fairall (1988) during his spectroscopic survey of bright nucleus galaxies. AM0530-421 has the highest blue luminosity in our sample (L_B =1.7 10^{11} $L_\odot$). It also has the highest HI

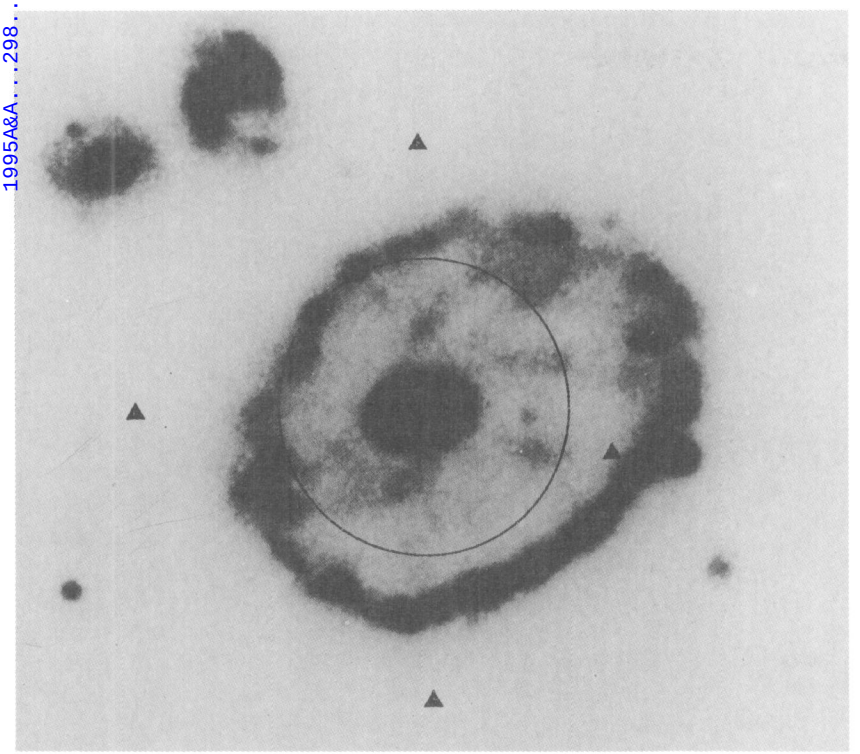

Fig. 5. Optical photograph of the Cartwheel (taken from AM). The circle indicates the resolution of the observations, the dark triangles the positions observed

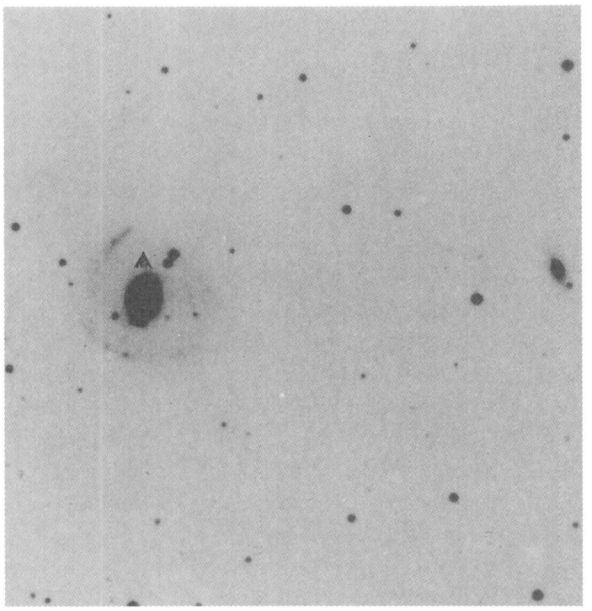

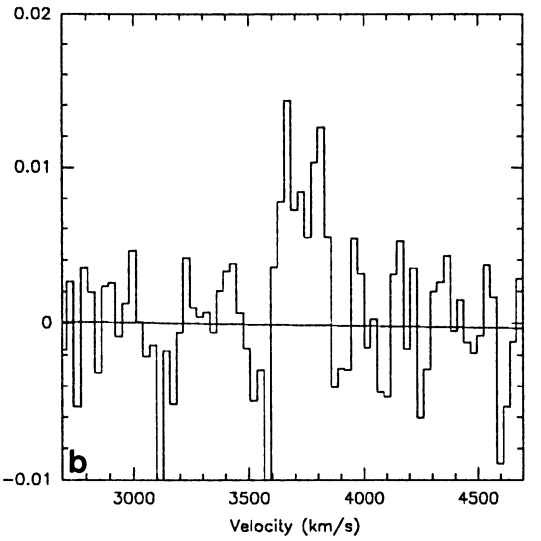

Fig. 6a. Optical photograph of AM1045-245 (taken from AM). **b** CO(1-0) spectrum of AM1045-245. The velocity resolution is 29.1 $\mathrm{km\,s^{-1}}$

mass (4.6 $10^{10}\,M_\odot$, see spectrum in Fig. 3c). We have mapped AM0530-421 in the CO(1-0) transition. Figure 3b shows the global spectrum. We derived an H_2 mass of 5.2 $10^9\,M_\odot$.

3.4. The Vela ring (AM1006-38; Sersic's ring)

The Vela ring is a distinctive object among ring galaxies, mainly because of its central bar which makes it resemble the greek letter θ (Fig. 4). This suggests that the progenitor was a barred galaxy, although one might wonder whether a bar would have survived the passage of a companion galaxy through the disk. Vela's morphology is complex (Dennefeld et al. 1979): there are three rings, with major axis diameters of 73"= 23kpc, 17"=5.4 kpc and 10"=3.2 kpc respectively, and two bars, one connecting the outer ring to the inner ring structures (with a position angle of 40°) and the second connecting the inner ring to the nucleus (with a position angle of 90°). A nearby elliptical galaxy is visible with close radial velocity (Δv= 336 $\mathrm{km\,s^{-1}}$). However, as

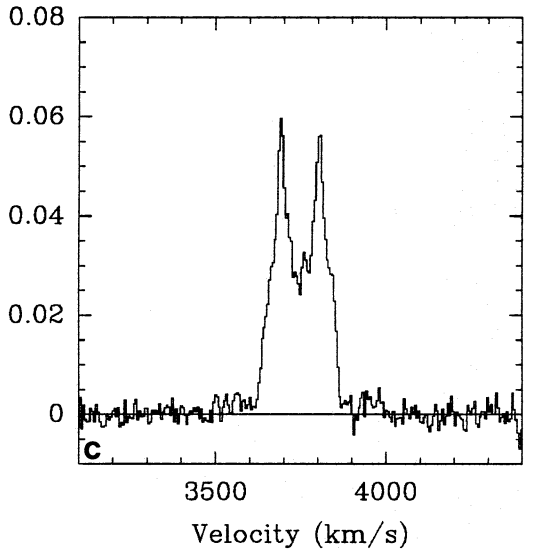

Fig. 6c. HI spectrum of AM1045-245 obtained with the Nançay radiotelescope. The velocity resolution is 5.3 $km\,s^{-1}$

pointed out by Taylor & Atherton (1984, hereafter TA84), the companion does not lie near the minor axis as usually observed and predicted by the models, but approximately 45 °away from it. The companion could have passed on a slightly hyperbolic orbit through the disk of the main galaxy. Vela's kinematics are complicated as well. TA84 have obtained a map of the Hα velocity field and found that the outer ring has an expansion velocity of 39 $km\,s^{-1}$ and almost no rotation (v_{rot}= 13 $km\,s^{-1}$). The outer ring rotates even more slowly than the inner one (v_{rot} = 15 $km\,s^{-1}$)! The dynamical mass derived from those velocities is thus extremely low: about 10^9 $M_\odot$.

We have mapped Vela in the CO(1-0) and CO(2-1) transitions and detected signal only at the centre position. Figure 4 shows that the CO(1-0) and CO(2-1) lines are extremely narrow (a gaussian fit yields 35 ± 6 and 28 ± 5 $km\,s^{-1}$ respectively) which is very unusual for a galaxy nucleus. Even galaxies seen almost face-on have linewidths of about 100 $km\,s^{-1}$. We know only one case (NGC 628) in which CO lines narrower than 50 $km\,s^{-1}$ have been observed (Braine et al. 1993). Those linewidths agree however with the rotational velocities observed by TA84.

The width of the HI line is less than 100 $km\,s^{-1}$ and the total HI mass is 7 10^8 $M_\odot$ (Dennefeld & Martin 1994), that is, about half that of the total molecular gas mass that we derive from the CO(1-0) observations ($M(H_2)$= 1.4 10^9 $M_\odot$). At the distance of 65 Mpc that we adopt for Vela, our 22" CO(2-1) beamwidth, which covers the innermost ring, corresponds to 7 kpc. Assuming that the CO lines are thermalized (I_{21}= I_{10}), we can derive an H_2 mass of 4 10^8 $M_\odot$ within that region, which is of the same order of the dynamical mass estimated by TA84 inside the inner ring radius. This is rather unusual, but the uncertainties on both the molecular and the dynamical masses are large (because of the use of the 2–1 transition and of the low inclination of the galaxy respectively). Nevertheless, a large fraction of the mass in the central regions of Vela is in molecular form, a characteristic which is often seen in mergers.

3.5. Cartwheel

The Cartwheel (A0035-34, ESO 350-G040) is a beautiful southern ring galaxy, which exhibits a large and bright outer ring connected to an inner ring by spokes (Fig. 5). It has three small elliptical companions located to the North-East, but the one that has collided with the Cartwheel and caused its present-day appearance remains unidentified. Indeed, no neighbour seems massive enough. Meanwhile, it is possible that the intruder has lost some of its mass during the encounter. The Cartwheel has been well studied in the optical (Theys & Spiegel 1976; Fosbury & Hawarden 1977) and in the near-infrared (Marcum et al. 1992, hereafter MAH92). The very blue colours of the outer ring shows that it has recently experienced a burst of star formation. The radial colour gradients discovered by MAH92 suggest that the starburst is more recent in the outer regions of the galaxy, which is coherent with the idea of a density-wave propagating outwards as in the simulations of Hernquist & Weil (1993). The Cartwheel has been detected in the far-infrared by the IRAS satellite and it has a far-infrared luminosity of 2.6 10^{10} $L_\odot$ and a (60 μm /100 μm) colour temperature of 33.3 K. Its HI mass is 3.3 10^{10} $M_\odot$ (Mebold et al. 1977).

We have observed the Cartwheel in the CO(J=1-0) line during several observing sessions at SEST. Because of the large angular size of the galaxy (more than 80" along the major axis) we have made a 5-point map with 45" sampling. We also observed the positions at offsets (-29", -7.7") and (-7.7", -29") which correspond to bright knots in the optical picture. None of these positions was detected. The total integration time on the galaxy is 34 hours (2033 minutes) and the r.m.s. noise in 30 $km\,s^{-1}$ channels 0.6 mK. The upper limit on the H_2 mass is then 1.5 10^9 $M_\odot$ if we take the HI linewidth (355 $km\,s^{-1}$, Mebold et al. 1977) and assume that the emission is extended on about 80 arcsec scale. This would in turn imply that the galaxy contains at least 20 times more atomic hydrogen than molecular hydrogen. Of all the sample galaxies for which the HI mass is known, the Cartwheel would have the lowest H_2/HI ratio.

Despite its prominent star formation activity, the CO emission of the Cartwheel is very low. This does not mean that it does not contain any molecular hydrogen. Indeed, the Cartwheel is found to be very deficient in heavy elements (Fosbury & Hawarden 1977). Oxygen, nitrogen and neon are lower by factors of 6, 22 and 3 when compared to the Orion nebula (in the Large Magellanic Cloud, oxygen is deficient by a factor 2 only and CO emission is weaker by a factor of 6, Cohen et al. 1988). MAH92 suggested that the progenitor of the Cartwheel could be a gas-rich low-surface brightness galaxy such as Malin 1, and that the disk of this galaxy is undergoing its first epoch of star formation. Indeed, there is no evidence of old stars in the outer ring (Marcum et al. 1992). The non-detection of CO emission could then be due to the low amount of CO molecules, because of the low metallicity, and not to the absence of molecular gas. However, the limit on the H_2 mass is not very good (this is due

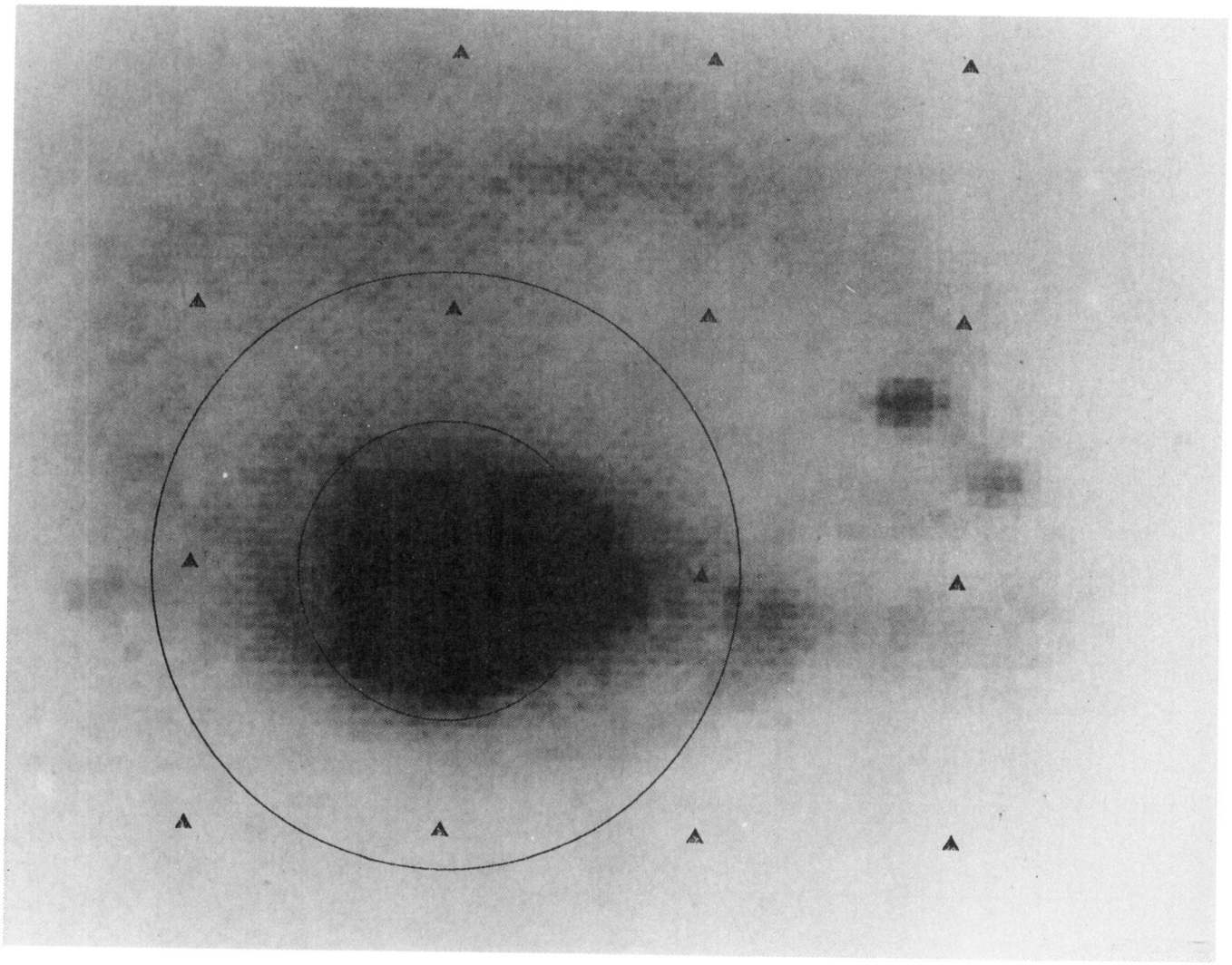

Fig. 7a. Optical photograph of NGC 985 (Rodriguez Espinoza & Stanga 1990). The circles indicate the resolution of the observations, the dark triangles the positions observed

to the large distance and angular size of the Cartwheel). The value of L_{FIR}/M(H_2) is not especially high (> 17.7) and the value of M(H_2)/L_B (< 0.024) is not especially low. Both are within the range where most galaxies are found (Horellou et al. 1994; Gerin et al. 1994; see Sect 4.1). It is thus difficult to reach definite conclusions concerning the molecular hydrogen content of the Cartwheel, and this disappointing case testifies the actual limitations of CO observations.

3.6. AM1045-245 (=NGC 3393= ESO 501-G10)

AM1045-245 is a Seyfert type 2 ring galaxy with a bright nucleus (Diaz et al. 1988; see Fig. 6a). We have detected a double horned CO(1-0) line towards the centre position but nothing at the position (0",45") (Fig. 6b).

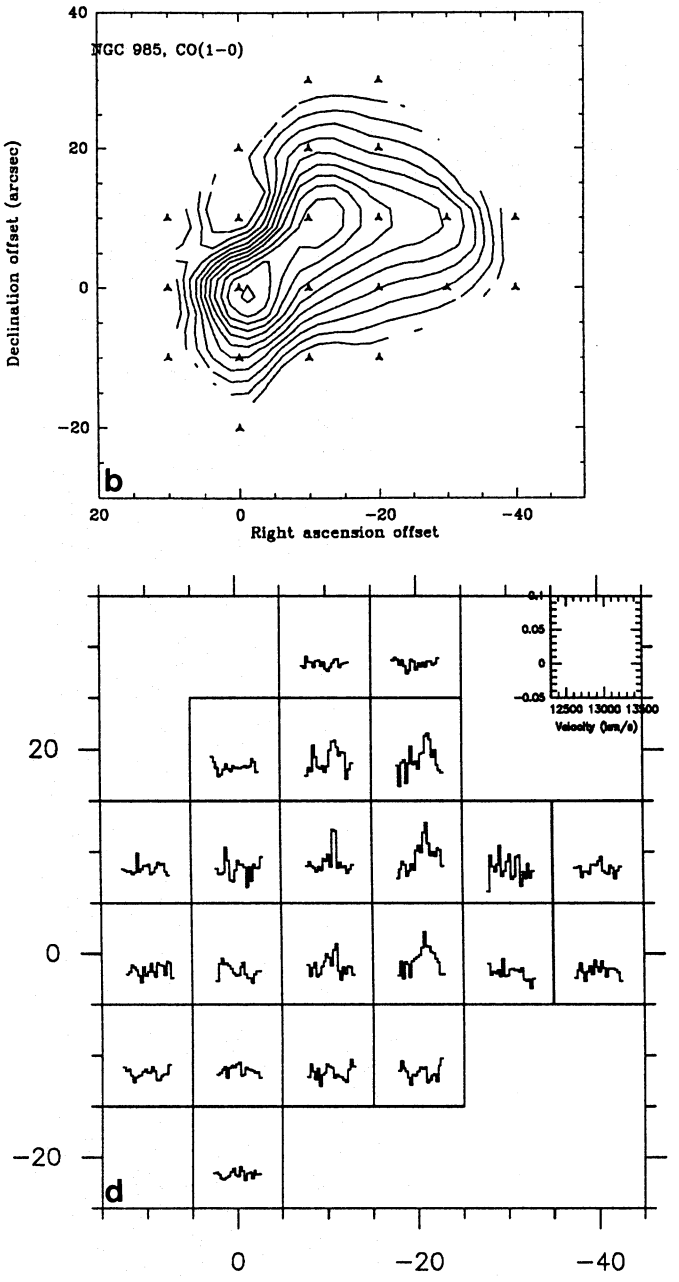

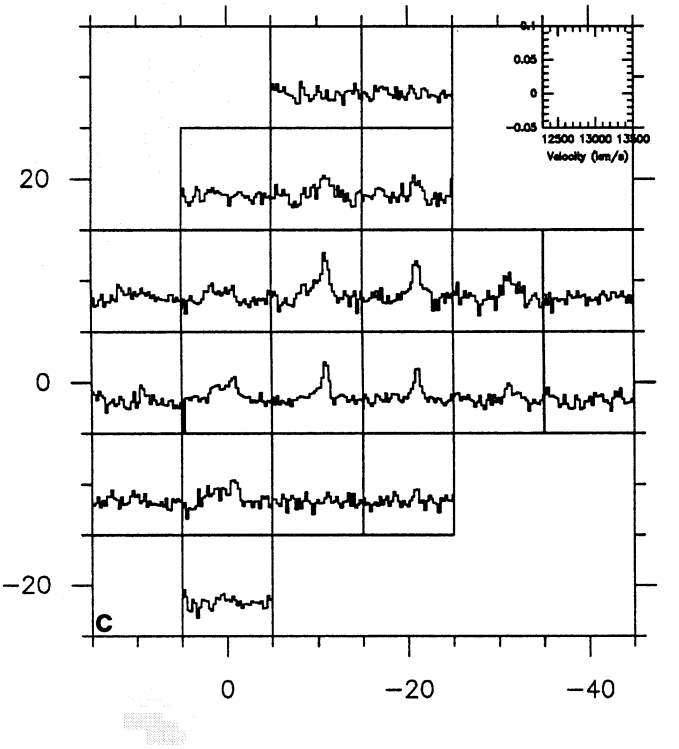

Fig. 7b. Contour map of the CO(1-0) emission of NGC 985. Levels between 1 and 12 K km s^{-1} by steps of 1 K km s^{-1}CO(1-0) spectra obtained toward NGC 985. The velocity resolution is 31.2 km s^{-1}. **d** CO(2-1) spectra obtained toward NGC 985. Same scale and velocity resolution as in **c**

3.7. NGC 985 (=Mrk1048,VV285)

NGC 985 (Fig. 7a) is one of the largest rings known (about 30 kpc diameter). It has no visible nearby companion but the bright knot seen in projection on the ring may be the intruder galaxy. Its light distribution follows an $r^{1/4}$ law typical of a nuclear bulge or an elliptical galaxy (Appleton & Marcum 1993, hereafter AM93). Moreover, near–infrared observations (AM93) reveal a second nucleus about 3" from the first one, from which the twisted western arm originates. That suggests that NGC 985 is a composite system of two galaxies and therefore fits into the class of collisional ring galaxies. The bright knot hosts a Seyfert 1 nucleus that largely contributes to the X-ray, UV and far-infrared emission of NGC 985 (Ghigo et al. 1983; Wu et al. 1983; Rodriguez Espinoza & Stanga 1990, hereafter R-ES90). Bright HII regions have been detected in the ring (R-ES90).

Figure 7c and d show the CO(1-0) and CO(2-1) spectra we have obtained and a contour map of the CO(1-0) emission. The grid spacing of our maps is 10", that is, half of the beamwidth for the CO(1-0) map and the beamwidth for the CO(2-1) map. We clearly detected both CO(1-0) and CO(2-1) emission at several positions in NGC 985. The CO(1-0) line at the centre position is very broad (600 km s^{-1} at the zero level) and has a double-horn profile. The two velocity components lie at 12740 km s^{-1} and 12975 km s^{-1}. In CO(2-1) no emission is detected at the centre position but narrow lines at the higher velocity are seen at the north-west. However, the 512 MHz bandwidth corresponds only to 666 km s^{-1} which prevents us from detecting the broad component. Alloin et al. (1992) have observed the central po-

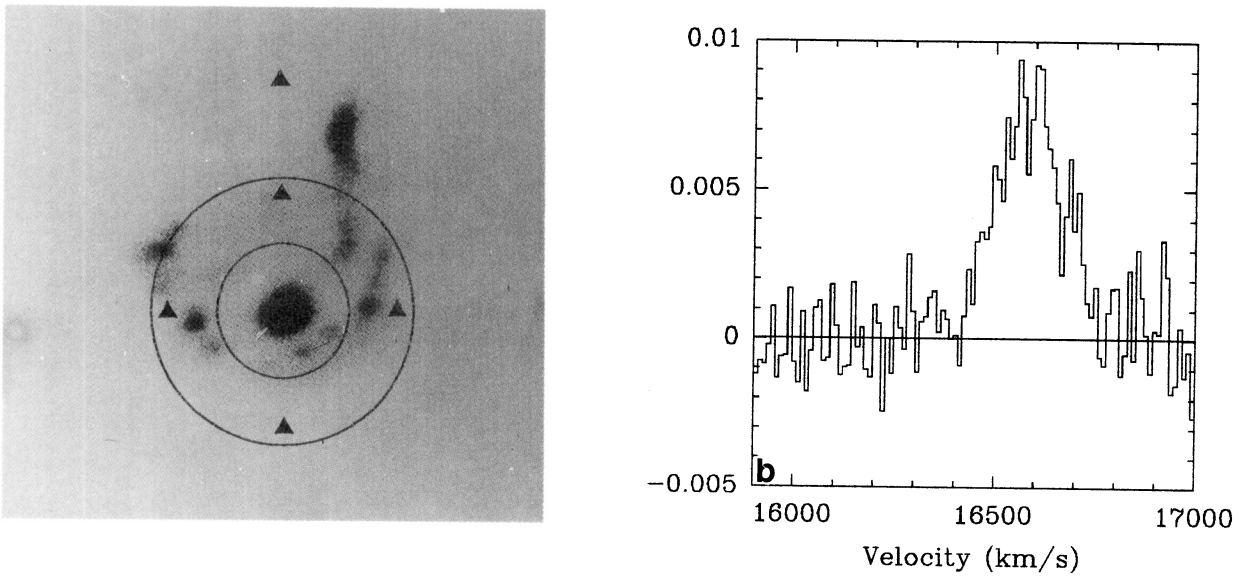

Fig. 8a. Optical photograph of the Sextans ring (the circles indicate the resolution of the observations, the dark triangles the positions observed) **b** HI spectrum of Sextans obtained with the Nançay radiotelescope. The velocity resolution is 10.6 km s^{-1}

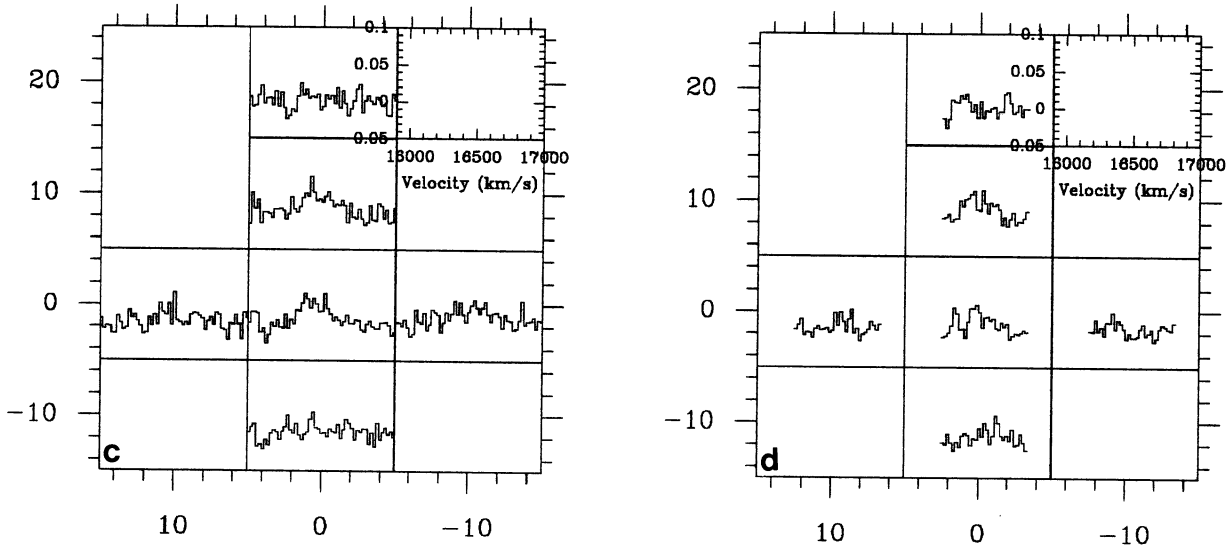

Fig. 8c. CO(1-0) map of the Sextans ring. The velocities range from 15 900 to 17 000 km s^{-1} and the main-beam temperatures from -0.05 to 0.1 K. The velocity resolution is 20.8 km s^{-1}. **d** CO(2-1) map. Same scale and velocity resolution as in **c**

sition of NGC 985 in ^{12}CO(2-1), also with the 30m telescope, and detected a narrow line, which corresponds to the one that we see at the (10",10") offset. We suspect that small pointing errors, or a misalignment between the 3mm and 1mm receivers, could explain this discrepancy. Alloin et al. also present a Kitt Peak CO(1-0) spectrum which exhibits a high velocity wing that we do not see in our data.

Figure 7b is a contour map of CO(1-0) emission. The maximum of emission corresponds to the galaxy nucleus. The emission is extended over the whole galaxy body although there are some indications that it is not directly associated with the ring seen in the near-infrared and Hα but rather with the inner regions.

We derived from the CO(1-0) observations a total H_2 mass of 1.2 10^{10} $M_\odot$, which is of the order of the H_2 mass in the merger remnant Arp 220 (Sanders & Mirabel 1985). Heckman et al. (1978) obtained an upper limit on the HI mass of 5.8 10^9 $M_\odot$. We have also observed NGC 985 in HI with the Nançay radiotelescope but did not detect any emission. This suggests a situation similar to that observed in mergers, in which the cold interstellar medium is mainly in the molecular phase.

3.8. Sextans ring (= IRAS 0959-0755)

This galaxy in Sextans is an incomplete knotty ring with an off-centre Seyfert 1 nucleus (Wakamatsu & Nishida 1987; see Fig. 8a). Its recession velocity is 16500 km s^{-1}. A small companion

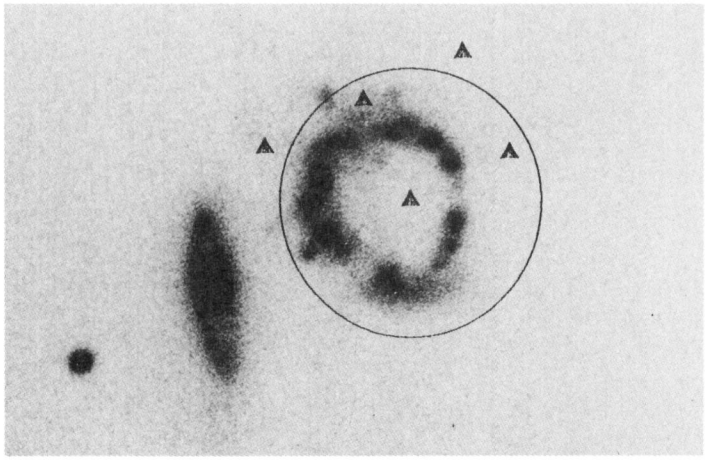

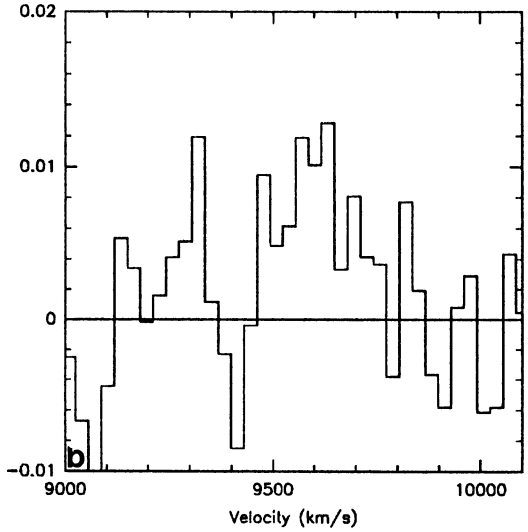

Fig. 9a. Optical photograph of Arp 147 (Arp 1966). **b** CO(1-0) spectrum of Arp 147. The velocity resolution is 31.2 km s^{-1}

galaxy located 17"NW of the nucleus seems to be connected to the ring. The velocity difference between the two galaxies is around 160 km s^{-1}. The system is one of the most luminous galaxies in the sample, with a far-infrared luminosity $> 10^{11}$ L$_\odot$.

We have mapped Sextans in the CO(1-0) and CO(2-1) lines and have detected CO(1-0) emission at the centre position and at 10" north of the nucleus (Figs. 8c and d). We derive a molecular gas mass of 1.1 10^{10} M$_\odot$, which corresponds to a very high M(H$_2$)/L_B ratio: 0.24, three times higher than the mean for the sample, and about ten times higher than galaxies in the comparison sample (Section 4.1).

3.9. Arp 147 (IC 298A)

Arp 147 is a well-known empty ring galaxy with a bright elongated companion (IC 298B) located near the minor axis (Fig. 9). The system has been studied by Jeske (1986) whose results can be summarized as follows: the companion has a systemic velocity 200 km s^{-1} lower than that of Arp 147. The ring contains many knots of HII regions in which Hα emission has been detected. HI has been detected both associated with the companion and Arp 147. The HI mass of Arp 147 itself is about 4 10^9 M$_\odot$ (Jeske 1986). We have mapped Arp 147 in the CO(1-0) line. Figure 9 shows the average spectrum. We derive an H$_2$ mass of about 2.2 10^9 M$_\odot$. We have not detected any CO(2-1) emission.

3.10. IIZw28

IIZw28 has no nearby companion visible, so the collisional origin of this galaxy could be in some doubt (picture in Sargent 1970). However, there is good evidence that IIZw28 has a buried companion in the ring. Indeed, the north side of the ring is very thick and Sargent (1970) detected Balmer absorption line at this position. The spectra obtained by Appleton and Marston (1994) show three distinct stellar populations: a)young stars in the ring, b)A-stars which are distributed insied the ring (this is strong evidence for the passage of the wave) and c) an old stellar population in the edge of the ring. It is thus very likely that the companion seen in projection like in NGC 985. The galaxy has been detected in HI by Jeske (1986) and it has M(HI)= 2.3 10^9 M$_\odot$. It was not detected by IRAS and we did not detect any CO emission. Our limit on the H$_2$ mass is 8 10^8 M$_\odot$.

3.11. IRAS20210+1121

IRAS20210+1121 is the most distant source in our sample, with a recession velocity of 16900 km s^{-1}. It is a type 2 Seyfert galaxy with a bright bulge inside an eccentric ring (Pérez et al. 1990; see Fig. 10). This galaxy is closely interacting with a companion at a projected distance of 1.1 kpc. It is the brightest infrared source of the sample and its far-infrared luminosity is 4 10^{11} L$_\odot$.

We have detected CO(1-0) and CO(2-1) emission in IRAS 20210+1121 (Fig. 10). The molecular hydrogen mass is 4.1 10^9 M$_\odot$. With a L_{FIR}/M(H$_2$) ratio larger than 80, this object can be compared to the most extreme mergers.

3.12. Arp 119 (Kar 29, VV 347, Mrk 983)

Arp 119 (Fig. 11) is usually not classified as a ring galaxy. It has an elliptical companion and an arc-like morphology with an extension in the direction of the companion. The striking point is that two systems with velocities different by several hundreds of km s^{-1} are coexistent in this galaxy. Indeed MB93 have found that the velocity of the nucleus is 14379 km s^{-1} while that of the knot of emission in the direction of the companion, at about 8" from the centre, is 15172 km s^{-1}, a result confirmed by the Hα observations of Marziani et al. (1994).

The observed characteristics of Arp 119 could be the consequence of a head-on collision with the companion. Using N-body simulations we have made a crude model of the encounter

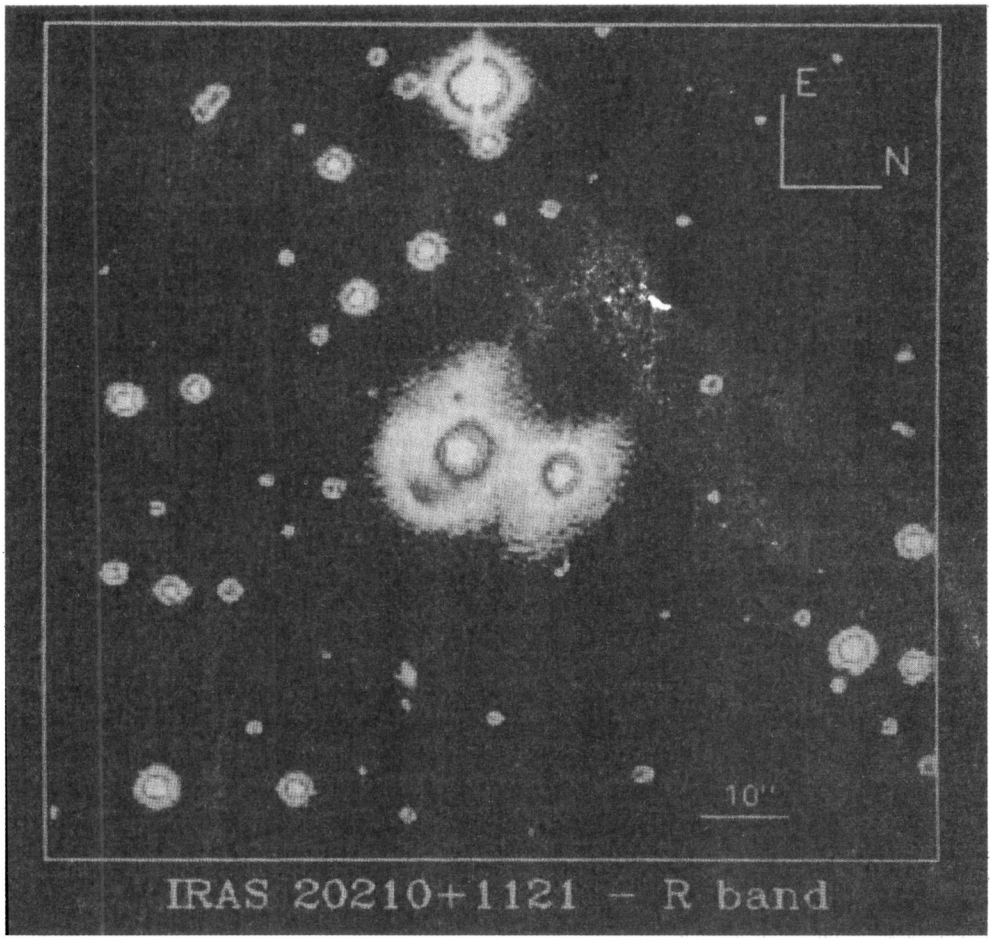

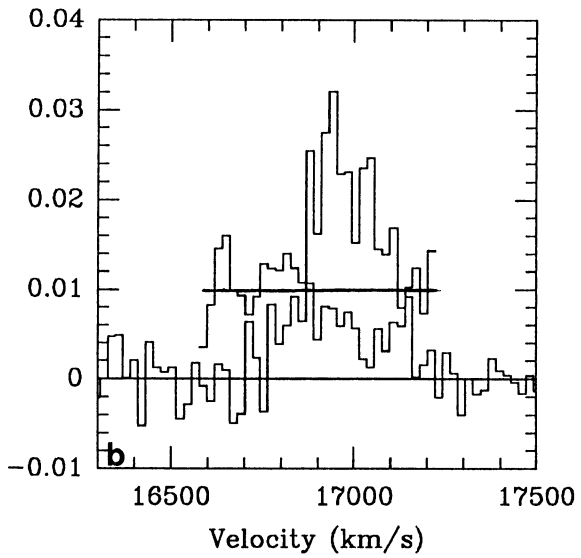

Fig. 10a. Grey scale image in the R band from IRAS20210 (Pérez et al. 1990). **b** Superposition of the CO(1-0) and CO(2-1) spectra (dark line, offset by 0.01 K for clarity). The velocity resolution is 20.8 km s^{-1} for both lines

with galaxies of equal masses (Horellou & Combes 1994). A ring visible in both the gaseous and stellar components develops immediatly after the passage of the elliptical companion through the disk. A second gaseous ring appears after about 1.5 10^8 years ; it lies in a different plane. The gas and stars behave differently, and gas is being expelled out of the galaxy. Although we have not tried to optimize the parameters to reproduce the observed morphology of Arp 119, this model explains some of the observed features: the gas outflow, the inner ring, and the bright arc which is actually a projection effect. These results show that it is likely that Arp 119 owes its morphology to the same processes as the other galaxies in the sample.

We have observed Arp 119 with the Arecibo telescope and the IRAM 30m telescope. Strong HI, CO(1-0) and (2-1) lines

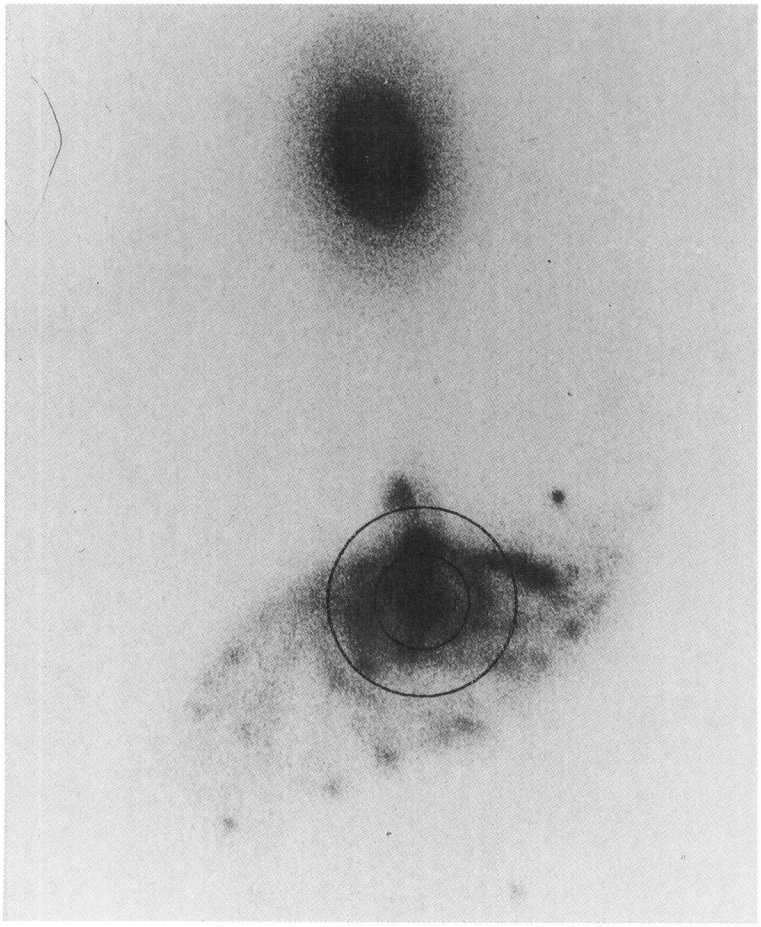

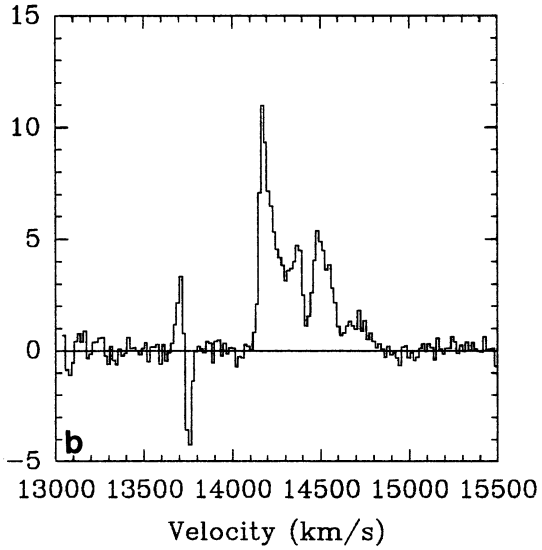

Fig. 11a. Optical photograph of Arp 119 (Arp 1966). **b** HI spectrum of Arp 119 obtained at Arecibo. The fluxes are in mJy, the velocity resolution is 16.5 km s^{-1}. The features around 13700 km s^{-1} are due to interferences

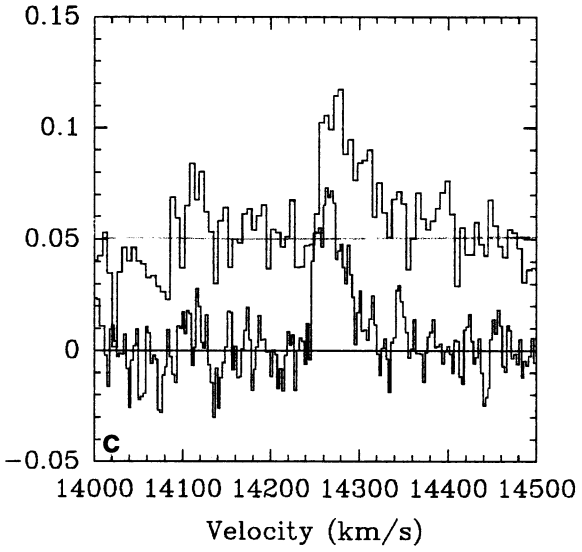

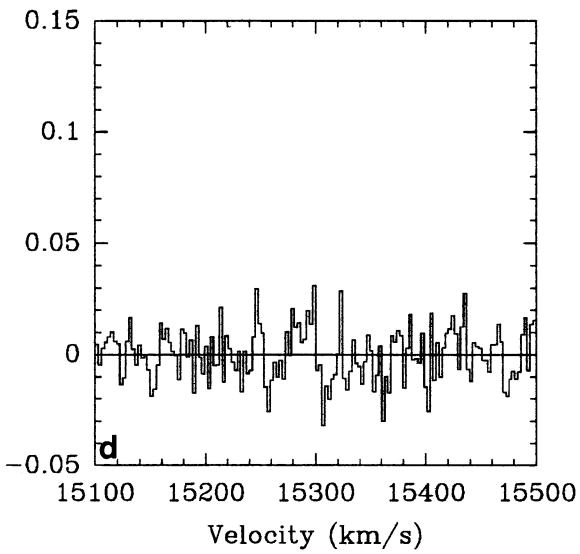

Fig. 11c. ^{12}CO(1-0) spectrum of Arp 119, observed with the IRAM 30m telescope superimposed onto the ^{12}CO(2-1) line (dark line, offset by 0.05K for clarity). The receiver frequency has been centered on the velocity of the main body, 14 265 km s^{-1}. The velocity resolution is 2.7 km s^{-1} for the ^{12}CO(1-0) line and 5.4 km s^{-1} for the ^{12}CO(2-1) one. **d** CO(1-0) spectrum obtained at the position of Arp 119 but with the receiver frequency centered on 15300 km s^{-1}, which is the velocity of the other system observed in Hα in Arp 119. The velocity resolution is 2.7 km s^{-1}

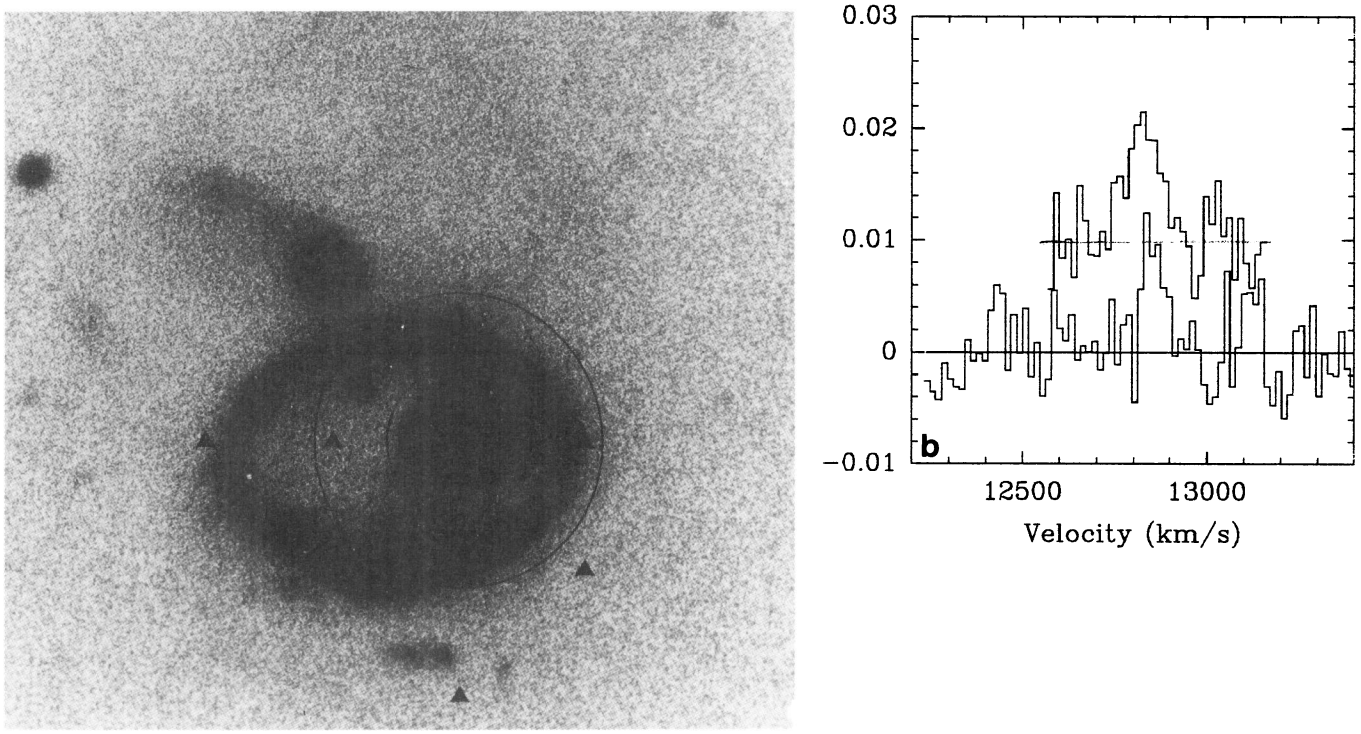

Fig. 12a. Optical photograph of IIHz4. **b** 9-point average CO(1-0) spectrum of IIHz4 and CO(2-1) spectrum (offset by 0.01K for clarity). The velocity resolution is 15.6 km s^{-1} for both lines

are detected at the velocity of the main body (Fig. 11). The corresponding molecular hydrogen mass within the 22" beam is 4 10^9 $M_\odot$ that is about 1/3 of the HI mass (1.2 10^{10} $M_\odot$). The observed 2-1/1-0 line ratio is about 1 ($\pm$ 0.2), but the beamsizes are different at the two frequencies. Considering that the 22" beam covers 20.6 kpc at the 193 Mpc distance of Arp 119, this is a rather large value for the line ratio (for example, the line ratios for galaxies in the Coma cluster at a velocity of 8000 km s^{-1} are lower than 1 (Casoli et al. 1991). The CO(2-1) spectrum is slightly broader and more structured than the CO(1-0) one but both are very narrow. The HI spectrum is very asymmetric with a lot of structure. Note the different widths of the HI and CO spectra: the CO(1-0) emission lies between the two first HI peaks (at 14150 and 14350 km s^{-1}). The HI component at about 14500 km s^{-1} is probably associated with the neighbour companion Mrk983 located about 2.5 arcmin from Arp 119 and has a similar recession velocity. Moreover, we have also observed Arp 119 with the Nançay radiotelescope whose beam is larger than that of the Arecibo telescope and this component is much stronger in the Nançay spectrum. The fourth component in the HI spectrum is the small bump that appears on the high-velocity side of the HI spectrum at about 14700 km s^{-1}. The atomic gas mass associated is about 9 10^8 $M_\odot$. It cannot be associated with a neighbour galaxy. Interferometric HI observations are necessary to determine the location of this gas.

What about the second velocity system (at about 15300 km s^{-1}) detected in Hα by MB93 and Marziani et al. (1994)? It is absent in the 21 cm data, and we did not detect it in the CO lines either (Fig. 11d). The upper limit for the H_2 mass at this velocity is 2.4 10^9 $M_\odot$ if the width of the emission is 100 km s^{-1} as in the main system. It seems unlikely that we have missed part of the CO emission because the 22" beam covers 20.6 kpc, and the spatial separation between the two components is only 8" (Mazzarella & Boroson 1993).

Both the atomic gas and molecular gas masses are rather normal for the blue luminosity of this galaxy (see Table 3). With an L_{FIR}/M(H_2) ratio of 18, Arp 119 is forming stars a little more efficiently than the other galaxies in the sample but it is far from being an ultraluminous galaxy.

3.13. IIHz4

IIHz4 (Fig. 12) has a recession velocity of about 12800 km s^{-1} and was not detected by IRAS. A long exposure photograph reveals the remarkable double ring morphology of this system that Lynds & Toomre (1976) were able to reproduce in their numerical simulations. Both rings are nearly perfect ellipses. The companion ring is much fainter and has an off-centre nucleus. The recession velocity difference between the two nuclei is 50 km s^{-1}, the primary nucleus having the higher velocity. A circular model fits the data of Lynds and Toomre for the primary ring and gives an inclination angle of 42°, a rotation velocity of 28 km s^{-1} and an expansion velocity of 44 km s^{-1}.

We have mapped IIHz4 in the CO(1-0) and CO(2-1) lines with 10" spacing. No clear line is visible at the individual positions. Figure 12 shows the CO(1-0) and CO(2-1) spectra obtained by averaging the individual spectra which shows that the CO emission is extended and diffuse. The CO(1-0) linewidth is

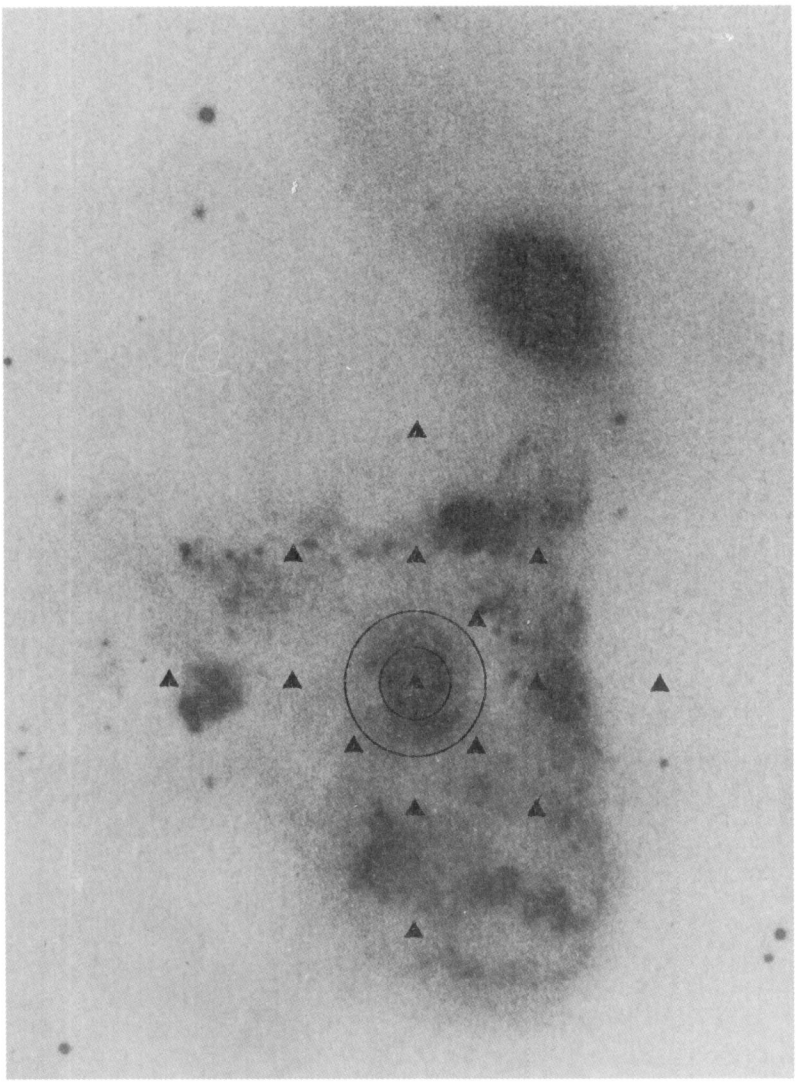

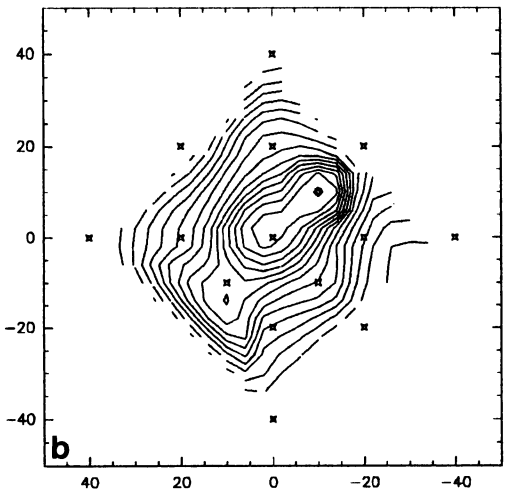

Fig. 13a. Optical photograph of Arp 143 (Arp 1966). **b** Contour map of the CO(1-0) emission of Arp 143, levels between 1 and 15 K km s^{-1} by steps of 1K km s^{-1}

62 ± 14 km s^{-1}. The HI line is about 100 km s^{-1} wide but the two galaxies were contained in the Arecibo beam (Jeske 1986). We derived an H_2 mass of 1.3 10^9 $M_\odot$ that is about five time less than the HI mass derived by Jeske for the whole system.

3.14. Arp 143 (=VV117= NGC 2444/5)

This galaxy was referred to as "the blue nest" by Vorontsov-Velaminov (1959). It has a highly disturbed aspect with many optical knots surrounding the nucleus (Fig. 13). The knots are

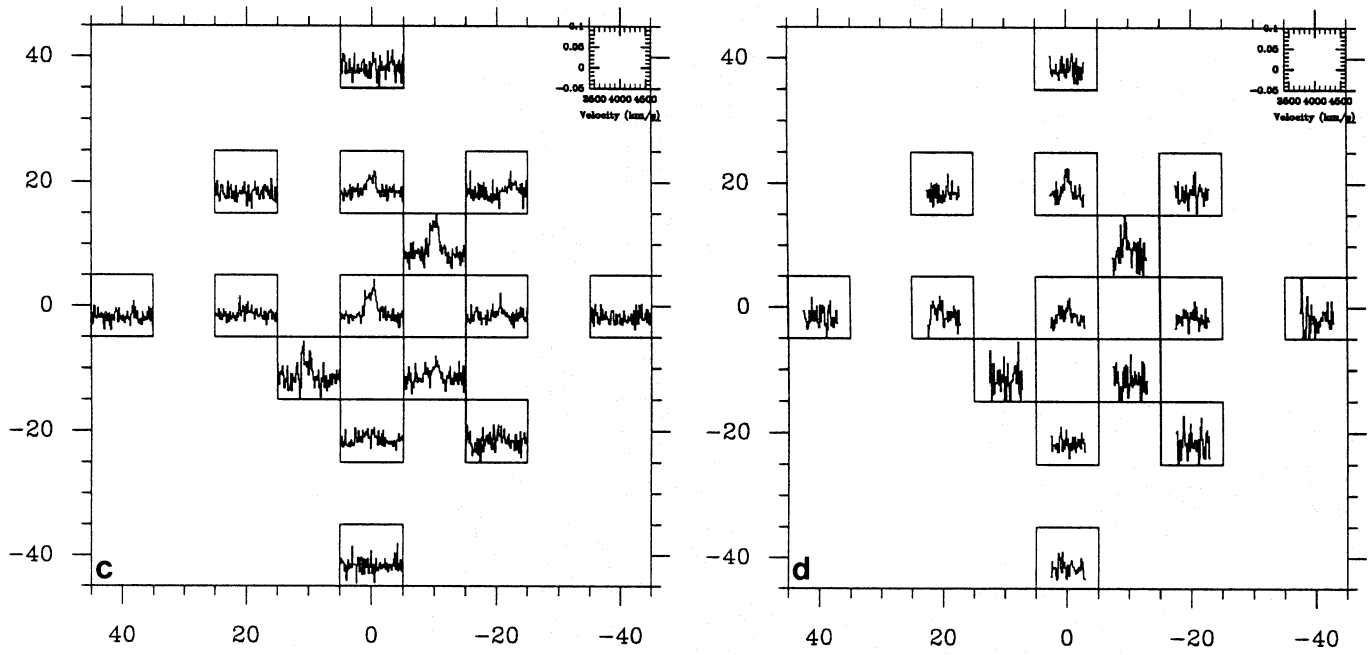

Fig. 13c. CO(1-0) map of Arp 143. The velocities range from 3400 to 4900 km s^{-1} and the main-beam temperatures from -0.05 to 0.1 K. The velocity resolution is 15.6 km s^{-1}. **d** CO(2-1) spectra obtained toward Arp 143. Same scale and velocity resolution as in **c**)

very blue and associated with HII regions and are probably young star clusters (Appleton et al. 1992). Appleton et al. (1987) detected an HI filament containing about 5 10^8 $M_\odot$ beginning to the north of the companion, NGC 2444, and extending up to 150 kpc to the north of the galaxy. We have mapped Arp 143 in the CO(1-0) and CO(2-1) transitions (Fig. 13c and d). The CO emission is extended since it is detected at 20" distance (5.2 kpc) from the centre. It is however much less extended than the HI emission mapped by Appleton et al. (1992) and CO emission is detected only at the positions where the HI column densities are larger than 4 10^{21} at cm^{-2}.The derived H_2 mass is 3 10^9 $M_\odot$ while the HI mass is 6.6 10^9 (Gallagher et al. 1981).

3.15. Arp 148 (= VV32, A1101+41= Mayall's Object)

Arp 148 (Fig. 14) is perhaps the strangest object in the sample. It consists of a ring and a cigarshape body perpendicular to it. The two components are separated by 12" and 250 km s^{-1} (Burbidge 1964). Arp 148 is very likely the result of a head-on collision and the companion is probably emerging from the ring or the two nuclei could be at an intermediate stage of coalescence (Joy & Harvey 1987). Arp 148 is a OH megamaser source (Martin 1989). Jeske (1986) detected nonthermal radio continuum emission at λ20 cm in the cigar.

We have mapped Arp 148 in the ^{12}CO(1-0) line (Fig. 14). At the (0,0) position which is at the centre of the elongated body, a broad line (300 km s^{-1}) is detected. Arp 148 is extreme in its absolute and relative molecular gas content, with M(H_2)= 1.2 10^{10} $M_\odot$ (the highest value in the sample with NGC 985) and M(H_2)/ L_B = 0.4 (the highest value in the sample). Its star formation activity is elevated (L_{FIR}/L_B = 9.4).

3.16. Arp 145

Arp 145 (Fig. 15a) appears as a wispy ring with an elliptical companion located near the minor axis. The two bright knots visible on the ring are foreground stars. We have mapped Arp 145 with the IRAM telescope (Fig. 15c). The emission is strongest at (-10,0). Figure 15c shows the average CO spectrum (full line) and the HI spectrum (dashed line) that we have obtained with the Nançay radiotelescope.

4. Global results

Out of the 16 ring galaxies that we have observed, we have detected 14 in the ^{12}CO(1-0) transition. HI masses are known for 12 ring galaxies. An overview of the results is given in Table 3.

4.1. Gas content

To compare observed quantities from one galaxy to another, we need to scale them to the mass or size of the object. Since the diameters at the 25th mag arcsec^{-2} isophote, D_{25}, of these disturbed objects are not well determined (and unknown in many cases) we have chosen to scale all quantities and in particular the molecular gas mass to the blue luminosity L_B .

To compare the gas content of ring galaxies with that of normal galaxies, we have used the distance-limited sample of 66 nearby galaxies observed in CO by Sage (1993a, hereafter S93; 1993b). Figure 16 shows the distributions of M(HI)/ L_B and M(H_2)/ L_B for this control sample and the ring galaxy sample. The average M(HI)/ L_B and M(H_2)/ L_B ratios for

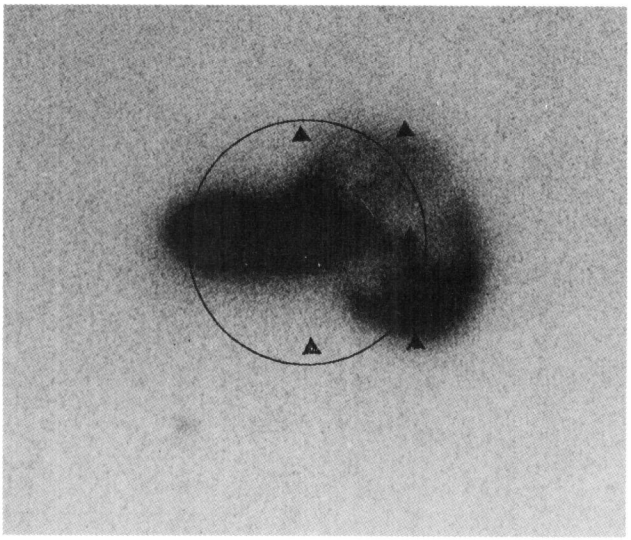

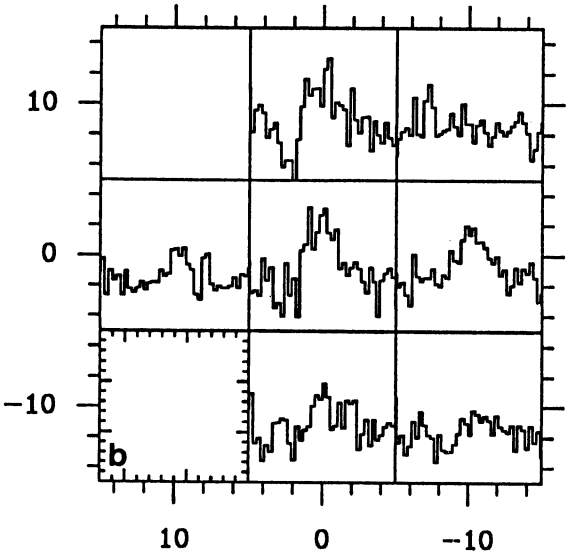

Fig. 14a. Optical photograph of Arp 148 (Arp 1966). **b** CO(1-0) spectra of Arp 148. The velocities range from 9800 to 11 000 km s^{-1} and the main-beam temperatures from -0.05 to 0.1 K. The velocity resolution is 31.2 km s^{-1}

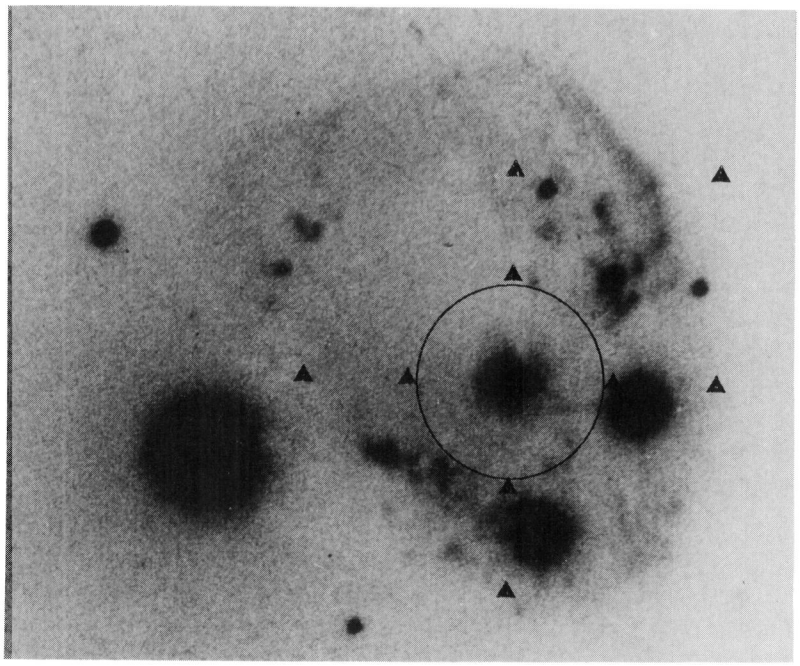

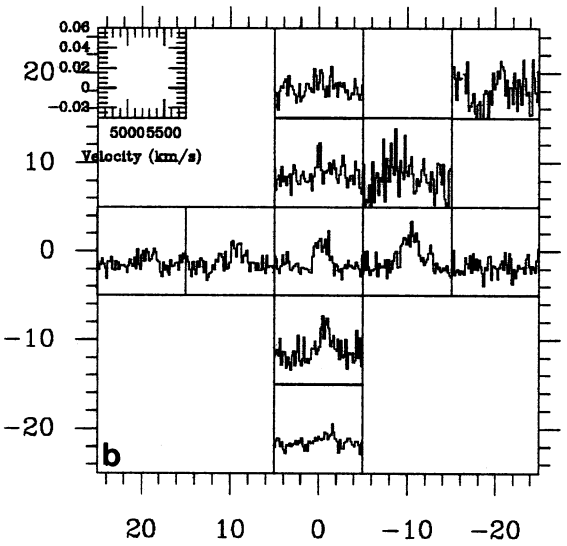

Fig. 15a. Optical photograph of Arp 145 (Arp 1966). **b** CO(1-0) spectra of Arp 145. The velocities range from 4600 to 5800 kms-1 and the main-beam temperatures from -0.03 to 0.06 K. The velocity resolution is 20.8 km s^{-1}

the control sample and and for the ring galaxies are listed in Table 4.

We have systematically computed either the mean or the median of the values, since they appear sometimes to be very different. For the control sample however, mean and average values are comparable. The value quoted in Table 4 includes the upper limits for $\log(M(H_2)/L_B)$. Excluding them yields an average value of -1.14 ± 0.41 (log(0.07)) which is not very different.

The atomic hydrogen content of ring galaxies is very comparable to that of the control sample. We have compared the two distributions using a t-test. The probability that the means are drawn from the same population is about 25%; this hypothesis cannot be excluded. Ring galaxies are neither HI-rich nor

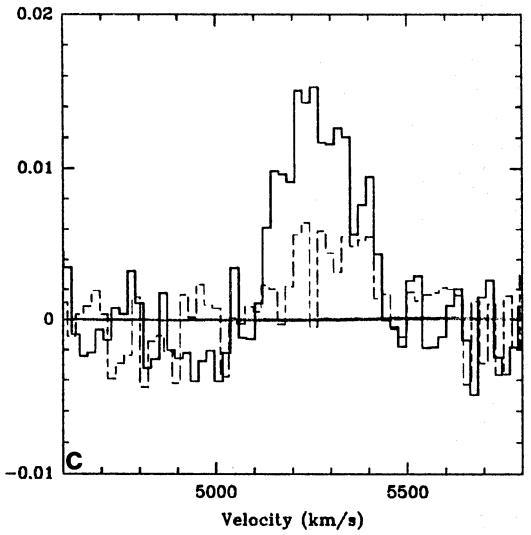

Fig. 15c. CO(1-0) spectrum of Arp 145 (full line) superimposed on the HI spectrum (dashed line) obtained in Nançay . The y-scale correspond to the main-beam temperature scale for the CO(1-0) spectrum and to T_A^* scale for the HI spectrum. The velocity resolution is 20.8 km s^{-1} for the CO(1-0) line and 21.1 km s^{-1} for the HI line

Table 4.

	log[M(HI)/ L_B]	log[M(H_2)/ L_B]
S93	-0.72 ± 0.56= log(0.19)	-1.58 ± 0.45= log(0.026)(ave)
	-0.61 ± 0.56= log(0.24)	-1.56 ± 0.45= log(0.027)(med)
Rings	-0.83 ± 0.47= log(0.15)	-1.18 ± 0.41= log(0.066) (ave)
	-0.82 ± 0.51= log(0.15)	-1.27 ± 0.41= log(0.054) (med)

Table 5.

	T_{dust}	log[L_{FIR}/ L_B]	log[L_{FIR}/M(H_2)]
S93	30.8 ± 3.8	-0.73 ± 0.37 = log(0.19)	0.86 ± 0.39 (ave) = log(7.2)
	30.6 ± 3.8	-0.74 ± 0.37 = log(0.18)	0.81 ± 0.39 (med) = log(6.5)
Rings	37.1 ± 6.9	0.01 ± 0.47 = log(1.02)	1.19 ± 0.29 (ave) = log(15.5)
	36.0 ± 6.9	-0.14 ± 0.49 = log(0.72)	1.21 ± 0.29 (med) = log(16.2)

HI-deficient. On the other hand, they are CO bright and H_2 rich compared to the control sample. Their H_2 content is more than twice as high as for the control sample galaxies. The probability that the means are drawn from the same population is less than 0.1%. The two samples are statistically different in their mean far-infrared and blue luminosities (<log(L_{FIR})>= 10.6 ± 0.4 for the rings and 9.0 ± 0.8 for S93; <log(L_B)>= 10.6 ± 0.3 for the rings and 9.6 ± 0.6 for S93). We have also compared our data with those of Combes et al. (1994) obtained for a sample of binary galaxies. This sample has mean values closer to ours: <log(L_{FIR})>= 10.4 ± 0.5 and <log(L_B)>= 9.9 ± 0.4. Binaries are also found to have a high molecular gas content, even slightly higher than that of ring galaxies (<log(M(H_2)/ L_B)>= -0.7 ± 0.5).

4.2. Star formation activity

Few observational data related to star formation are available for ring galaxies. The only parameters that exist for the whole sample are the far-infrared fluxes obtained by IRAS. The far-infrared luminosity of a galaxy is partly due to the reemission by dust grains of the UV emission of massive stars; it can be therefore be used as an indicator of the recent star formation activity. Meanwhile, this is clearly not the best measure since dust heated by the interstellar radiation field as well as active nuclei also contribute to the far-infrared emission.

From the IRAS fluxes at 60 and 100 μm , we have computed far-infrared luminosities L_{FIR} and colour temperatures T_{dust} for the ring galaxies and the control sample (Tables 1 and 2). The far-infrared luminosities and the far-infrared to blue luminosity ratio L_{FIR}/L_B are higher for ring galaxies, as shown on Fig. 17: all ring galaxies lie in the upper right part of the plot. The two objects with highest far-infrared luminosity and L_{FIR}/L_B are IRAS20210+1121 and Arp 148.

Table 5 presents the average and median values of T_{dust}, log(L_{FIR}/L_B) and log(L_{FIR}/M(H_2). The colour temperatures and log(L_{FIR}/L_B) of ring galaxies are significantly higher than those of the control sample. This confirms the results of Appleton & Struck-Marcell (1987a): ring galaxies have a higher level of star formation than normal galaxies.

Not surprisingly, the far-infrared luminosity correlates with the H_2 mass (Fig. 18). Again, the higher infrared luminosities and molecular gas masses of the ring galaxies are visible on this plot. Note that these are normalized quantities since they have been divided by L_B.The correlation is better with the molecular gas mass alone than with the total gas mass content (HI+ H_2)/ L_B. This result has been found by several authors for larger samples (e.g., Young et al. 1989). This suggests that the molecular gas rather than the atomic gas is linked to star formation, at least as it is revealed by the far-infrared emission. The star formation efficiency as measured by the ratio of the far-infrared luminosity and the molecular gas mass L_{FIR}/M(H_2) is higher for ring galaxies than for galaxies of the control sample (Table 5). Of course, it would be of great interest to compare other indicators of star formation such as the UV emission, the Hα emission or the radiocontinuum emission with each other and with the CO and FIR emission. Unfortunately, such data are not available for ring galaxies yet.

5. A related class: Hoag-type objects

We have also searched for CO emission in two Hoag-type objects: Hoag's object itself (see Fig. 19) and NGC 6028. Both exhibits two-horned HI lines typical of rotating disks (Schweizer et al. 1987; Giovanelli et al. 1981); the widths of the HI lines are 240 and 275 km s^{-1} which seem large for objects apparently seen almost face-on. The derived HI masses are 8 10^9

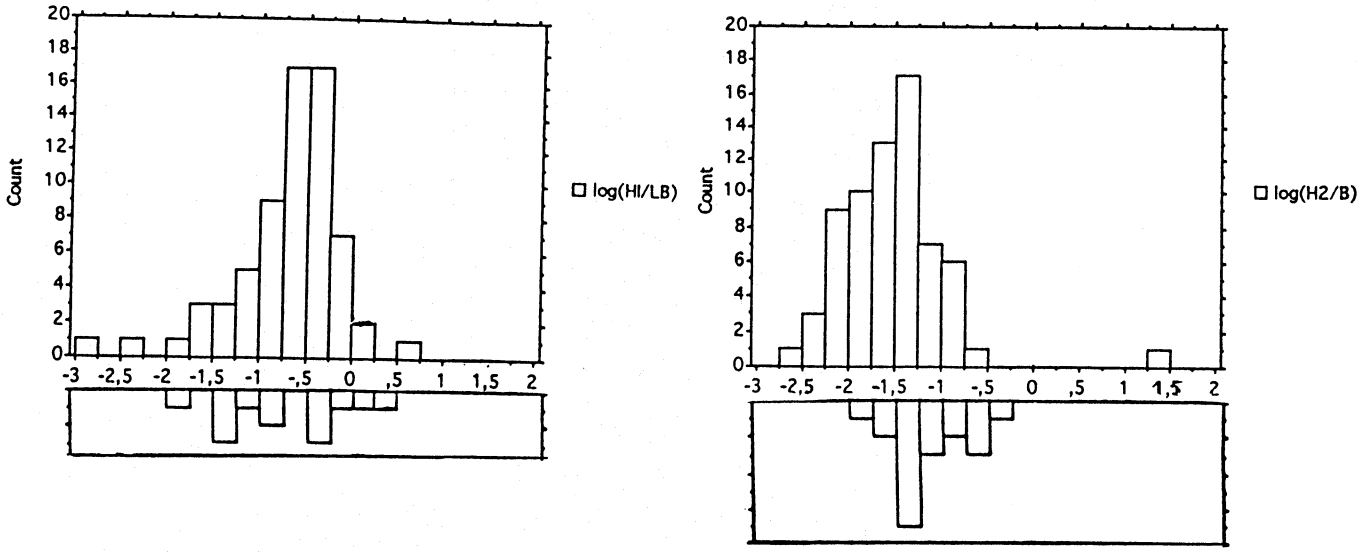

Fig. 16. Histogram of the values of log(M(HI)/ L_B) and log(M(H_2)/ L_B) for the ring galaxies (in negative) and the galaxies of the comparison sample (Sage 1993a, b)

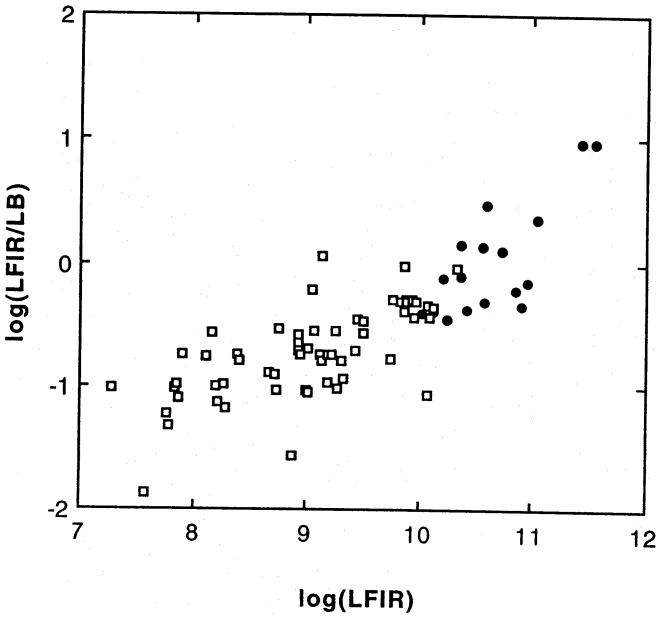

Fig. 17. L_{FIR}/L_B versus L_{FIR} for the ring galaxies (black dots) and the galaxies of the comparison sample (squares) (Sage 1993)

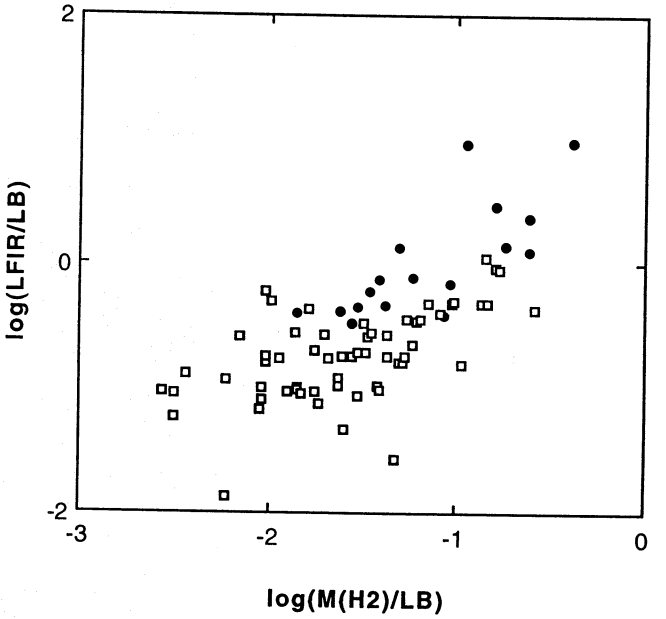

Fig. 18. L_{FIR}/L_B versus H_2/L_B for the ring galaxies (black dots) and the galaxies of the comparison sample (squares) (Sage 1993a, b)

$M_\odot$ and 1.6 10^9 $M_\odot$ respectively. Surprisingly, Brosch (1985) did not detect any HI emisssion using the Westerbork Synthesis Radiotelescope at the position of Hoag's Object, although the mass estimated by Schweizer et al. is 4 times larger than the WSRT upper limit for a non detection. This suggests that the atomic hydrogen is diffuse and extends over a 20 arcsec scale (the synthesized beamsize of the WSRT observations was about 12") which would be in agreement with the model of an accreted disk (Schweizer et al. 1987).

We have not detected CO in either Hoag's object or in NGC 6028. Our upper limits on the H_2 masses are 7 10^8 and 4.5 10^7 $M_\odot$ these are 30 and 10 times less that the HI masses respectively. If Hoag-type objects are polar ring galaxies, they are expected to have very little molecular gas in the core (an early-type galaxy) and the whole H_2 would be in the ring and therefore difficult to detect.

6. Conclusions

The detection rate of ring galaxies in the ^{12}CO(1-0) transition is high: out of 16 ring galaxies observed, 14 have been detected. Moreover, ring galaxies are bright in CO compared to normal galaxies whereas their HI emission is not statistically different.

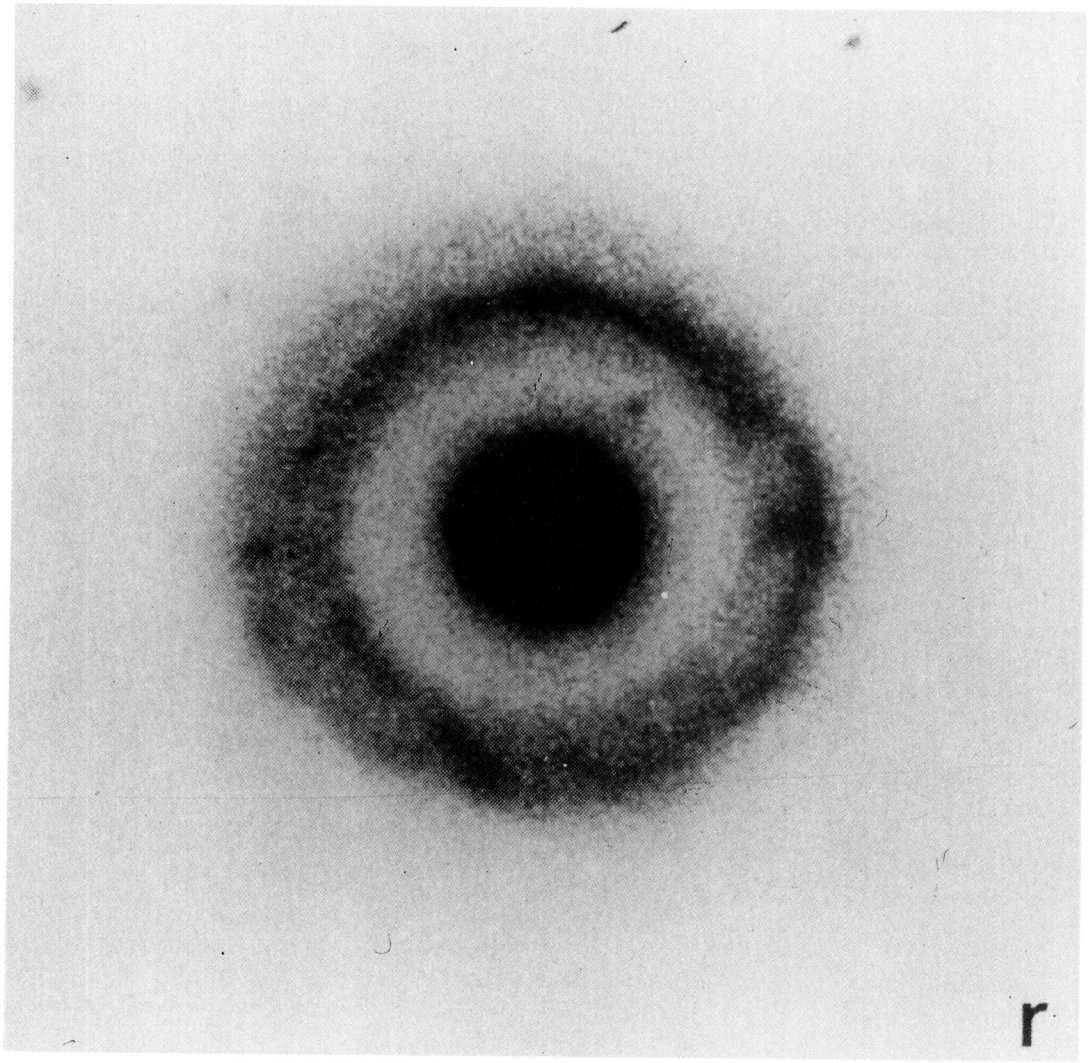

Fig. 19. Optical photograph of Hoag's object (Schweizer et al. 1987)

Using the factor determined in our galaxy to convert CO emissivities into H_2 column densities we have derived large molecular gas masses. This suggests that a large amount of material is available for star formation. This result is in agreement with the higher star formation rate of ring galaxies compared to isolated ones, as derived from their higher far-infrared luminosities and far-infrared to blue luminosity ratios.

Of the two galaxies not detected in CO, one is IIZw28 which was detected by IRAS at 60 μm only. The other case of non detection is the Cartwheel galaxy. We suggest that the weak CO emission of this galaxy is due to its low metallicity. The CO observations do not exclude the possibility that the Cartwheel is H_2 rich and actively forming stars.

In our survey, narrow CO lines appeared rather frequently. This may indicate a bias of our sample towards low inclination galaxies. Moreover, narrow lines are detected more easily than broad ones.

The fraction of ring galaxies with a Seyfert nucleus is high in our sample (4 out of 19 objects). Could the interaction have been relevant for the onset of Seyfert activity? In the scenario proposed by Sanders et al. (1988) the flow of gas towards the nucleus would be favoured by interactions, thus contributing to the infall of gas at the rate needed to maintain the Seyfert activity, according to the models that assume an accretion disk around a black hole as the central energy source of Seyfert galaxies. We have detected elevated CO emission in three out of the four Seyfert ring galaxies of the sample. Large gas quantities could thus fuel the Seyfert nucleus. Heckman et al. (1989) have found that Seyfert 2 galaxies have a significantly higher $M(H_2)/L_B$ ratio whereas Seyfert 1 galaxies are normal. This does not appear clearly in our sample.

We have detected CO at the centre position of several ring galaxies (Vela, IC 4448) but not in the ring. In IIHz4 we have found evidence that the CO emission is extended. Observations with higher sensitivity and higher resolution will be possible in the future and will allow to locate more precisely the origin of the CO emission. Interferometric HI observations of some

objects would be very useful to locate the atomic gas and would be a great constraint to the models.

Acknowledgements. We gratefully thank the IRAM, SEST and Nançay staffs for their assistance during the observations, and J.-M. Martin for communicating us HI fluxes prior to publication. Special thanks to R. Giovanelli for having made the HI observations of Kar29 at Arecibo. We thank M. Gerin for having made some of the CO observations and E. Troup for his help during the observations at Parkes. We are grateful to L. Sage for valuable comments on the manuscript. We have used the SIMBAD database from the Centre de Données de Strasbourg (France) to retrieve bibliographic data, as well as the NASA Extragalactic Data Base (NED), and the Lyon Extragalactic Data Base (LEDA), to retrieve bibliographic and photometric data.

References

Alloin, D., Barvainis, R., Gordon, M.A., Antonucci, R.R.J., 1992, A&A 265, 429
Appleton P.N., Struck-Marcell C., 1987a, ApJ 312, 566 (IRAS data)
Appleton, P.N., Ghigo, F.D., van Gorkom, J.H., Schombert, J.M., Struck-Marcell, C., 1987, Nature, 300, 12, 140
Appleton, P.N., Schombert, J.M., Robson, E.I., 1992, ApJ 385, 491
Appleton, P.N., Marcum, P.M., 1993, ApJ 417, 90
Appleton, P.N., Marston, 1994, ApJ, preprint
Arp H.C., 1966, Atlas of Peculiar Galaxies, Pasadena, California Insititue of Technology
Arp , H.C., Madore B.F., 1987: A Catalogue of Southern Peculiar Galaxies and Associations, Cambridge University Press
Booth R.S., Delgado G., Hagström M., Johansson L.E.B., Murphy D.C., Olberg M., Linström C.O., Rydberg A., 1989, A&A 216, 315
Braine, J., Combes, F., Casoli, F., Dupraz, C., Gérin, M., Klein, U., Wielebinski, R., Brouillet, N., 1993, A&A 272, 754
Brosch, N., 1985, A&A 153, 199
Burbidge, E.M., 1964, ApJ 140, 1617
Buta, R., 1986: ApJ Suppl Series 61, 609, 26-A13
Casoli F., Boissé, P., Combes, F., Dupraz, C., 1991, A&A 249, 359
Cohen, R.S., Dame, T.M., Garay, G., Montani, J., Rubio, M., Thaddeus, P., 1988, ApJ 331, L95
Combes, F., Prugniel, P., Rampazzo, R., Sulentic, J.W., 1994, A&A 281, 725
Davoust, E., Considère, S., Poulain, P., 1991, A&A 252, 69
Dennefeld, M., Laustsen, S., Materne, J., 1979, A&A 74, 123
Dennefeld, M., Martin, J.-M., 1994, in prep for A&A
Diaz, A.I., Prieto, M.A., Wamsteker, W., 1988, A&A 195, 53
Fairall, A.P., 1988, MNRAS 233, 691F
Few, J. M. A., Madore, B.F., Arp , H.C., 1982, MNRAS 199, 633
Fosbury, R.A.E., Hawarden, T.G., 1977, MNRAS 178, 473
Fouqué, P., Bottinelli, L., Durand, N., Gouguenheim, L., Paturel, G., 1990, A&A Suppl. Series 86, 473
Gallagher, J.S., Knapp, G.R., Faber, S.M., 1981, AJ 96 1781
Ghigo, F.D., Wardle, J.F.C., Cohen, N.L., 1983, AJ 88, 1587
Giovanelli, R., Chincarini, G.L., Haynes, M., 1981, ApJ 247, 383
Gordon, D. Gottesman, S.T., 1981, AJ 86, 161
Graham, J.A., 1974, Observatory 94, 290
Heckman, T.M., Balick, B., Sullivan, W.T., 1978, ApJ 224, 745
Heckman, T.M., Blitz, L., Wilson, A.S., Armus, L., Miley, G.K., 1989, ApJ 342 735
Hernquist, L., 1989, Nature 340, 31
Hernquist, L., Weil, M.L., 1993, MNRAS 261, 804
Hoag, A.A., 1950, A.J. 55, 70
Horellou C., Casoli F., Dupraz C., Kazès, I., 1994, in preparation for A&A (Fornax galaxies)
Horellou, C., Combes, F., 1994, in N-body problems and gravitational dynamics, Proceedings of a Meeting held at Aussois, Eds F. Combes and E. Athanassoula, p. 168
Jeske N., 1986, PhD thesis, University of Berkeley, California.
Joy, M., Harvey, P.M., 1987, ApJ 315, 480
Laustsen, S., Madsen, C., West, R.M.: 1987, Exploring the Southern Sky, (ESO) Springer-Verlag, Berlin, Heidelberg
Lindsay, E.M., Shapley, H., 1960, Observatory, 80, 223
Londsdale, C.J., Helou, G., Good, J.C., Rice, W., Fullmer, L., 1989, Catalogued galaxies and quasars observed in the IRAS survey, Version 2, (Pasadena, JPL)
Lynds, R., Toomre, A., 1976, ApJ 209, 382
Marcum, P.M., Appleton, P.N., Higdon, J.L., 1992, ApJ 399, 57
Martin, J.-M., 1989, PhD thesis, Université de Paris VII
Marziani, P., Keel, W.C., Dultzin-Hacyan, D., Sulentic, J.W., 1994, "Kar29: Tidal effects from a second or third party", in "Mass-Transfer Induced Activity in Galaxies", Ed. I. Shlosman, Cambridge Univ. Press, p396
Mazzarella J.M., Boroson T.A., 1993, ApJS 85, 27 (MB93)
Mebold, U., Goss, W.M., Fosbury, R.A.E., 1977, MNRAS 180, 11P
Noguchi, M., Ishibashi, S., 1986, MNRAS 219, 305
Pérez, E. Manchado, A., Garcia-Lario, P., Pottasch, S.R., 1990, A&A 227, 407
Rodriguez Espinosa, J.M., Stanga, R.M., 1990, ApJ 365, 502
Sage, L.J., 1993a, A&A 272, 123
Sage, L.J., 1993b, A&ASS 100, 537
Sanders, D.B., Mirabel, F., 1985, ApJ 298, L31
Sanders, D.B., Soifer, B.T., Elias, J.H. et al., 1988, ApJ 325, 74
Sargent, W., 1970, ApJ 160, 405
Schweizer, F., Ford, W.K., Jr., Jedrzejewski, R., Giovanelli, R., 1987, ApJ 320, 454
Strong, A.W., Bloemen, J.B.G.M., Dame, T.M., Grenier, I.A., Hermsen, W., 1988, A&A 207, 1
Struck-Marcell, C., Appleton, P.N., 1987, ApJ 323, 480
Taylor, K., Atherton, P. D., 1984, MNRAS 208, 601
Theys, J.C., Spiegel, E.A., 1976, ApJ 208, 650
Theys, J.C., Spiegel, E.A., 1977, ApJ 212, 616
Vaucouleurs, de, G., Vaucouleurs, de, A., Corwin, H.G. Jr., Buta, R.J., Paturel, G., Fouqu'e, P., 1991, (RC3), Third Reference Catalogue of Bright Galaxies, Springer-Verlag
Vorontsov-Velaminov, B.A., 1959, Atlas and Catalogue of Interacting Galaxies Part I (Moscow: Moscow Univ. Press)
Wakamatsu, K., Nishida, M.T., 1987, ApJ 315, L23
Wakamatsu, K., 1990, ApJ 348, 448
Wu, C.C., Bogges, A., Gull, T.R.: 1983, ApJ 266, 28
Young, J.S., Xie, S., Kenney, J.D.P., Rice, W.L., 1989, ApJ Suppl. Series 70, 699
Zwicky, F., Herzog, E., Wild, P., Karpowicz, M., Kowal, C.T., 1961–1968, Catalog of Galaxies and Clusters of Galaxies, Pasadena: California Institute of Technology

This article was processed by the author using Springer-Verlag TEX A&A macro package 1992.